AGU PUBLICATIONS

JGR

Journal of Geophysical Research: Oceans

RESEARCH ARTICLE

10.1002/2016JC012592

Special Section:
Oceanic Responses and Feedbacks to Tropical Cyclones

Impact of sea spray on the Yellow and East China Seas thermal structure during the passage of Typhoon Rammasun (2002)

Lianxin Zhang[1,2], Xuefeng Zhang[1,3], P. C. Chu[4], Changlong Guan[5], Hongli Fu[1], Guofang Chao[1], Guijun Han[1], and Wei Li[1]

[1]Key Laboratory of State Oceanic Administration for Marine Environmental Information Technology, National Marine Data and Information Service, State Oceanic Administration, Tianjin, China, [2]Fisheries and Oceans Canada, Bedford Institute of Oceanography, Dartmouth, Canada, [3]College of Automation, Harbin Engineering University, Harbin, China, [4]Naval Ocean Analysis and Prediction Laboratory, Department of Oceanography, Naval Postgraduate School, Monterey, California, USA, [5]Physical Oceanography Laboratory, Ocean University of China, Qingdao, China

Abstract Strong winds lead to large amounts of sea spray in the lowest part of the atmospheric boundary layer. The spray droplets affect the air-sea heat fluxes due to their evaporation and the momentum due to the change of sea surface, and in turn change the upper ocean thermal structure. In this study, impact of sea spray on upper ocean temperatures in the Yellow and East China Seas (YES) during typhoon Rammasun's passage is investigated using the POMgcs ocean model with a sea spray parameterization scheme, in which the sea spray-induced heat fluxes are based on an improved Fairall's sea spray heat fluxes algorithm, and the sea spray-induced momentum fluxes are derived from an improved COARE version 2.6 bulk model. The distribution of the sea spray mediated turbulent fluxes was primarily located at Rammasun eye-wall region, in accord with the maximal wind speeds regions. When Rammasun enters the Yellow sea, the sea spray mediated latent (sensible) heat flux maximum is enhanced by 26% (13.5%) compared to that of the interfacial latent (sensible) heat flux. The maximum of the total air-sea momentum fluxes is enhanced by 43% compared to the counterpart of the interfacial momentum flux. Furthermore, the sea spray plays a key role in enhancing the intensity of the typhoon-induced "cold suction" and "heat pump" processes. When the effect of sea spray is considered, the maximum of the sea surface cooling in the right side of Rammasun's track is increased by 0.5°C, which is closer to the available satellite observations.

Key Points:
- Sea spray parameterization scheme
- The distribution of the sea spray mediated turbulent fluxes was primarily located at Rammasun eye-well region
- The sea spray plays a key role in enhancing the intensity of the typhoon-induced "cold suction" and the "heat pump" processes

Correspondence to:
G. Han,
guijun_han@126.com

Citation:
Zhang, L., X. Zhang, P. C. Chu, C. Guan, H. Fu, G. Chao, G. Han, and W. Li (2017), Impact of sea spray on the Yellow and East China Seas thermal structure during the passage of Typhoon Rammasun (2002), *J. Geophys. Res. Oceans*, *122*, 7783–7802, doi:10.1002/2016JC012592.

Received 5 FEB 2017
Accepted 19 APR 2017
Accepted article online 9 JUN 2017
Published online 10 OCT 2017

© 2017. American Geophysical Union. All Rights Reserved.

1. Introduction

Under low wind speed conditions, the turbulent fluxes are always at the air-sea interface through the ocean-atmosphere interaction processes, which are called the interfacial turbulent fluxes. Under strong winds of severe weather systems (typhoon, hurricane, etc.), the large amounts of sea spray droplets are generated by wave breaking [*Zhang et al.*, 2011, 2012] in whitecaps and whipping spume from the tips of wave. The sea spray droplets can dramatically affect air-sea turbulent fluxes by modifying mean state of the air-sea interface. The interfacial turbulent fluxes are usually determined through using the Coupled Ocean-Atmosphere Response Experiment (COARE) version 2.6 bulk flux algorithm [*Andreas et al.*, 2008]. However, the traditional COARE algorithm does not include the parameterizations of heat and momentum fluxes induced by the sea spray.

The sea spray parameterization schemes have been developed to affect heat fluxes for several decades. *Riehl* [1954] first suggested that the sea spray evaporation can provide significant amount of heat in the air-sea interface. Based on the sea spray observation in a wind-wave tank, *Wu* [1974] showed that the magnitude of the sea spray evaporation contains 13% of the total evaporation by estimating the evaporation of sea spray for 13.4 m/s wind speed. *Zhang and Lou* [1995] and *Lou and Zhang* [1995] proposed empirical expressions of spray heat fluxes and water vapor fluxes through analyzing the physical processes of individual sea spray droplet. *Hasse* [1992] simply estimated the spray's impact using three distinct arguments: the total surface area of sea spray droplet, the energy constraint, and the evaporation implied by the sea-salt aerosol. The above methods are so complicated as to prevent them from being applied for practical use in estimating the sea spray mediated heat fluxes. Subsequently, based on the cloud microphysical equations, *Andreas* [1989, 1990, 1992, 1994], *Andreas et al.* [1998], and *Andreas and Mahrt* [2016], developed the bulk microphysical model to estimate the contribution of sea spray to the sensible and latent heat fluxes, and

pointed out that the heat fluxes induced by the sea spray became significant fractions of air-sea interfacial fluxes for the wind speed condition above 11–13 m/s. However, the valid wind speed of Andreas's sea spray heat fluxes parameterization only reaches 32 m/s. Based on the Andreas's parameterization, *Fairall et al.* [1994] obtained a new sea spray generation function (hereafter referred as FA94 scheme) including the wind speed and whitecap to improve the sea spray heat fluxes parameterization, with reasonable calculation of heat fluxes induced by sea spray in high wind speed condition (typhoon, hurricane, etc.). However, Fairall's sea spray algorithm ignores the feedback mechanisms between the sea spray and air-sea interface completely. In addition, the sea spray evaporation zone scale height and the whitecap areal fraction are user input parameters.

Similarly to the thermal effect of sea spray, sea spray droplets also affect the mean dynamic state of the surrounding air-sea interface, which further modifies the air-sea momentum exchange. It has been proved that the drag coefficient levels off and even decreases at high wind speeds [*Emanuel*, 1995; *Powell et al*., 2003; *Jarosz et al*., 2007; *Soloviev et al*., 2014]. *Powell et al*. [2003] proposed that the sea spray could significantly influence the momentum transfer for the wind speed above 34 m/s. *Makin* [2005] modified the logarithmic wind profile by introducing the influence of sea spray droplets, and proposed the sea spray mediated sea surface dynamic roughness length in high wind speed condition. This relation can predict the reduction of the drag coefficient for the wind speed exceeding the hurricane force, which agrees well with *Powell et al*.'s [2003] measurements under high winds. It should be mentioned that this relation regards the Charnock parameter as a constant, which is not suitable for low-moderate wind speed condition. Hence, the sea surface dynamic roughness length proposed by *Makin* [2005] should be expanded to consider the effect of sea spray from the low-moderate to high wind speed condition in the study, by which the effect of sea spray on momentum flux transfer at the air-sea interface is taken into account.

Associated with the parameterizations of sea spray, the numerical simulations of the effect of sea spray during typhoon and hurricane passages were reported. The atmosphere model, ocean model, and coupled air-sea model were employed to unveil the physical processes of the effect of sea spray on the typhoon and hurricane [*Uang*, 1999; *Meirink and Makin*, 2001; *Wang et al*., 2001; *Bao et al*., 2000; *Perrie et al*., 2005; *Jeffrey and William*, 2008]. Despite the effects of heat fluxes induced by sea spray were demonstrated by numerical simulations, very few studies attempted to consider the momentum effect of sea spray. In addition, the atmospheric model simulation showed the effects of sea spray on the hurricane intensity and track. But few of the previous studies tried to analyze the effect of sea spray on the response of the upper ocean during typhoons passage. To investigate the effect of sea spray on air-sea turbulent fluxes and upper ocean response, *Zhang et al*. [2015a,2015b] first to include the momentum and heat effect of sea spray into the General Ocean Turbulent Model to investigate the effect of sea spray on the upper ocean during typhoon passage. They indicated that sea spray acted as an additional source of air-sea turbulent fluxes and improved the response of upper ocean. However, the principal limitations of their studies were the use of the 1-D ocean model, which meant that horizontal advection and other associated physical processes were neglected.

To overcome the limitation of 1-D model, the three-dimensional POMgcs with thermal and dynamic effects of sea spray is used to investigate the overall impact of turbulent fluxes induced by sea spray on the midlatitude upper oceans during the typhoon passage. The effects of sea spray are divided into two physical processes. On the heat aspect, the FA94 sea spray parameterization is modified by adding the sea spray feedback mechanisms and the parameters that are more accord with the physical processes. On the momentum aspect, a new sea surface dynamic roughness length is proposed for full wind speed conditions for the open ocean where the dynamic effects of sea spray are introduced. As a pilot study, we choose the typhoon Rammasun to explore the effects of sea spray using the numerical simulations.

The remainder of this paper is organized as follows: the POMgcs model configuration, air-sea fluxes parameterization, and parameterization of the effect of sea spray are presented in section 2. Experiment design is described in section 3. The numerical results and discussions are presented in sections 4 and 5, respectively. The conclusion is given in section 6.

2. Model Description

2.1. The POMgcs Model

The POMgcs is a primitive equation, time-dependent, free surface, and coast ocean circulation model with Mellor-Yamada turbulence closure developed by *Blumberg and Mellor* [1987] and *Ezer and Mellor* [2004]. The ocean model is run for the domain covering the Yellow and East China Seas (YES) from 24°N to 41°N and

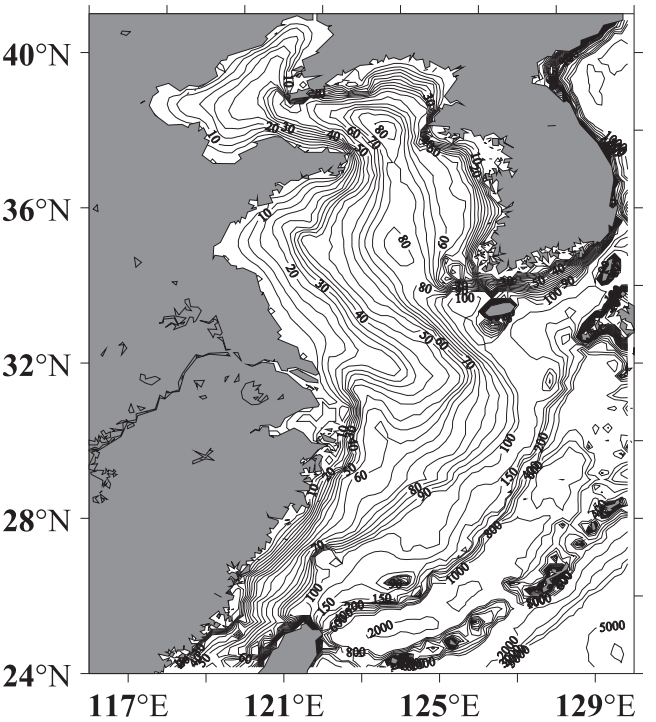

Figure 1. Model domain and isobaths.

from 116°E to 130°E (Figure 1), with a horizontal resolution of 1/6° and 35 layers in the vertical. The hybrid coordinate system is used, following the topography with sigma-level grid near a sloping bottom and *z*-level grid above the sigma level. The internal-mode and external-mode time steps are 600 and 10 s, respectively. The model initial and lateral boundary conditions of velocity, temperature, and salinity are derived from the China Ocean Reanalysis (CORA), which provides the reanalysis products of China coastal and adjacent seas from 1986 to 2013 [*Han et al.*, 2011]. The surface boundary condition including mechanical and thermal forcing [*Chu et al.*, 2000; *Chu and Cheng*, 2007]

$$\frac{K_M}{D}\left(\frac{\partial U}{\partial \sigma},\frac{\partial V}{\partial \sigma}\right)=-(<wu(0)>,<wv(0)>), \tag{1}$$

$$\frac{K_H}{D}\left(\frac{\partial T}{\partial \sigma}\right)=-(<w\theta(0)>)=\alpha_\theta\left(\frac{Q_H}{\rho_a c_{pa}}\right), \tag{2}$$

where the right-hand side of (1) is the air-sea turbulent momentum flux (i.e., wind stress). U and V are the velocity components. T is the potential temperature. Q_H is surface net heat fluxes (downward positive). K_M and K_H are the vertical mixing coefficients for momentum and tracers, respectively. c_p is the specific heat of air at constant pressure. ρ_a is the air density. The air-sea turbulent fluxes are calculated by sea-air parameters, which include the wind speed, the air temperature, the ocean temperature, the air humidity, the sea level pressure, etc. The wind data are interpolated from a new Cross-Calibrated, Multi-Platform (CCMP) ocean surface wind product, which is produced by combining all ocean surface wind observations from the SSM/I, AMSRE, and TMI, and all ocean surface wind vector observations from the QuikSCAT and SeaWinds. The spatial resolution is 0.25°. The air temperature, the ocean temperature, the air humidity, and the air pressure are obtained from the National Centers for Environmental Prediction (NCEP), whose temporal resolution and spatial resolution are 6 h and 1.899° × 1.875°, respectively. Also, the calculation of total air-sea momentum and heat fluxes is based on the COARE version 2.6 bulk flux algorithm, which is described below.

2.2. Air-Sea Fluxes Parameterizations

To provide the external forcing for POMgcs, the COARE version 2.6 bulk model is used to calculate air-sea interfacial turbulent momentum and heat fluxes, with the feedback processes between the sea surface temperature and air-sea turbulent fluxes. The air-sea momentum (M), sensible heat (H_S), and latent heat (H_L) fluxes are calculated by

$$M=\rho_a C_d U_{z_l}^2, \tag{3a}$$

$$H_S=\rho_a c_{pa} C_h U_{z_l}(\theta_0-\theta_{z_l}), \tag{3b}$$

$$H_L=\rho_a L_v C_k U_{z_l}(q_0-q_{z_l}), \tag{3c}$$

where U is the mean horizontal wind speed; θ is the potential temperature; q is the specific humidity; L_v is the latent heat of vaporization of water; the subscript "0" denotes the water surface, while z_l refers to the lowest level of the COARE bulk model. The drag coefficient (C_d), heat transfer coefficient (C_h), and

moisture transfer coefficient (C_k) are determined by the Monin-Obukhov similarity (MOS) for the constant flux layer

$$C_d = c_{dn} \Big/ \left[1 - \frac{c_{dn}^{1/2}}{\kappa}\psi_u(\xi)\right]^2 \tag{4a}$$

$$C_h = c_{Tn}^{1/2} c_{dn}^{1/2} \Big/ \left(\left[1 - \frac{c_{Tn}^{1/2}}{a\kappa}\psi_h(\xi)\right]\left[1 - \frac{c_{dn}^{1/2}}{\kappa}\psi_u(\xi)\right]\right) \tag{4b}$$

$$C_k = c_{qn}^{1/2} c_{dn}^{1/2} \Big/ \left(\left[1 - \frac{c_{qn}^{1/2}}{a\kappa}\psi_h(\xi)\right]\left[1 - \frac{c_{dn}^{1/2}}{\kappa}\psi_u(\xi)\right]\right), \tag{4c}$$

where κ is the von Karman constant (0.4). a accounts for the difference in scalar and velocity von Karman constants, and ψ is the MOS profile function. c_{dn}, c_{hn}, and c_{kn} are the transfer coefficients in the neutral conditions

$$c_{dn} = \frac{\kappa^2}{\ln^2(z_l/z_0)}, \tag{5a}$$

$$c_{Tn} = \frac{\kappa^2}{\ln(z_l/z_0)\ln(z_l/z_{0t})}, \tag{5b}$$

$$c_{qn} = \frac{\kappa^2}{\ln(z_l/z_0)\ln(z_l/z_{0q})}, \tag{5c}$$

where z_0, z_{0t}, and z_{0q} are the roughness lengths for velocity, temperature, and humidity. The roughness Reynolds number (R_r) is defined to characterize the surface and flow regimes

$$R_r = \frac{u_* z_0}{v}, \tag{6}$$

where v is the atmospheric kinematic viscosity. Similarly, the roughness lengths for temperature and humidity are defined by

$$z_{0t} = \frac{R_t v}{u_*}, \tag{7a}$$

$$z_{0q} = \frac{R_q v}{u_*}, \tag{7b}$$

with R_t and R_q are corresponding roughness Reynolds numbers, which are the functions of R_r.

The *Charnock* [1955] relation is used to calculate the sea surface dynamic roughness length

$$z_0 = \frac{\alpha_c u_*^2}{g}, \tag{8}$$

where g is the gravitational acceleration. a_c is the Charnock constant, and is set to 0.011 [*Fairall et al.*, 1996]. The Charnock relation works well to link the roughness length to the turbulent fluxes for the low-moderate winds with the surface wind speed up to 10 m/s [e.g., *Fairall et al.*, 1996]. When the wind speeds reach 10–15 m/s, the sea spray starts to affect the turbulent fluxes significantly [*Andreas*, 2010]. Thus, the effect of sea spray droplets is not included in the original version 2.6 COARE model, which can be used to calculate the interfacial turbulent fluxes (the turbulent fluxes that exclude (include) the effects of sea spray are called the interfacial (total) turbulent fluxes). Since the interfacial turbulent fluxes are nearly linear with the wind speed, the original COARE version 2.6 remains accurate for the calculation of the turbulent fluxes in the condition of the higher wind speeds after adding the sea spray effect.

2.3. Parameterization of the Effect of Sea Spray

2.3.1. Parameterization of Thermal Effect of Sea Spray

The FA94 is used to represent the sea spray mediated heat fluxes in this study, and it is developed based on the earlier work on sea spray droplet microphysics and the associated timescales of sea spray droplet [*Andreas*, 1989, 1992]. The sea spray mediated sensible heat flux contribution Q_s is proportional to the mass flux $\rho_w W S_v$

$$Q_s = S_v W \gamma(u) \rho_w c_{pw} (T_s - T_a), \tag{9}$$

where S_v and W are all the relevant whitecap normalized droplet volume fluxes and the whitecap areal fraction, respectively. $T_s - T_a$ is the air-ocean temperature difference. ρ_w and c_{pw} are the density and specific heat of liquid water, respectively. The sea spray mediated latent heat flux contribution Q_l is proportional to the total surface area of sea spray droplets per unit area of sea surface

$$Q_l = S_a h_d W \gamma(u) \beta(T_a) \rho_a L_e [q_s(T_a) - q], \tag{10}$$

where h_d is the evaporation zone scale height. Based on the *Hasse* [1992] sea spray heat fluxes model, S_a is set to 0.125 s^{-1} (given by FA94). $q_s(T_a)$ and q are the saturation mixing ratio and the ambient specific humidity, respectively. L_e is the latent heat of condensation. The sea spray droplets are maintained at the welt bulb temperature rather than the air temperature, thus the exchange term $\beta(T_a)$ is used

$$\beta(T_a) = \left[1 + \frac{0.622 L_e^2}{R c_{pa} T_a^2} q_s(T_a)\right]^{-1}. \tag{11}$$

Besides, $\gamma(u)$ represents the correction factor that exchanges the T_a and q from the mean wave height (h) to 10 m

$$\gamma(u) = 1 - 0.087 \ln \frac{10}{h}. \tag{12}$$

The numerical simulations show that the limited constant is about 0.5 [*Rouault and Larsen*, 1990; *Rouault et al*., 1991]. Incorporating equations (11) and (12) into equations (9) and (10) with a simple algebra, the final expressions for the sea spray mediated fluxes are then

$$Q_s = 0.5 S_v W \gamma(u_{10}) \rho_w c_{pw} (T_s - T_a), \tag{13a}$$

$$Q_l = 0.5 S_a h_d W \gamma(u_{10}) \beta(T_a) \rho_a L_e [q_s(T_a) - q], \tag{13b}$$

where both the sea spray evaporation zone scale height h_d and the whitecap areal fraction W(u) are controversial, thus this study focuses on the analysis of h_d and W(u).

First, h_d is crudely defined as the height above the mean sea surface below which 67% of the total droplet evaporation takes place. For simplicity, FA94 takes the mean wave height h to be the equilibrium wave height, which is a known function of the wind speed

$$h = 0.015\ u_{10}^2. \tag{14}$$

However, *Makin* [2005] suggested that the height of suspension layer of sea spray is higher (lower) than that of the breaking (significant) wave height, and set it to 1/10 of the significant wave height. Thus, 1/10 of the significant wave height is taken for the evaporation zone scale height of sea spray in the study. Significant wave height data are derived from European Center for Medium-Range Weather Forecasts (ECMWF).

Second, FA94 used the strong dependence of the wind speed on the whitecap areal fraction [*Monahan and Muircheartaigh*, 1980], obtained from the combined bubble droplet source function of *Miller* [1988] and the spume droplet function of *Wu et al*. [1984]

$$W = 3.8 \times 10^{-6} u^{3.4}. \tag{15}$$

However, the whitecap areal fraction does not only depend on the wind speed, but also on the state of wave and surrounding environment. *Zhao and Toba* [2001] found that the whitecap coverage from various data sources could be best fitted with the breaking-wave parameter

$$R_B = \frac{u_*^2}{\nu\omega_p}, \tag{16}$$

where ω_p is the angular frequency at the wave spectral peak. The whitecap coverage increases with R_B as follows [*Guan et al.*, 2007]

$$W = 3.88\times10^{-7}R_B^{1.09}, \tag{17}$$

which shows that the whitecap coverage does not only depend on the state of waves but also on the friction velocity. Therefore, equation (17) describes the comprehensive air-sea interfacial physical environment where the sea spray produces, and is used to calculate the whitecap areal fraction in the study.

2.3.2. Parameterization of the Dynamic Effect of Sea Spray

On the basis of open ocean observations, *Zhang et al.* [2015a,2015b] proposed a sea surface dynamic roughness z_0 with the effect of sea spray for the full wind speeds. It combines the Donalen relation and the resistance law of *Makin* [2005] by using the 3/2 power law [*Toba*, 1972] and the relation between the significant wave period and the peak wave period

$$z_0 g/u_*^2 = 0.0847^{(1-1/\omega)}\beta_*^{3(1-1/\omega)/2}n^{1/\omega}\beta_*^{m/\omega}, \tag{18}$$

which is called the Sea Spray Parameterization Scheme with containing the effect of sea spray and avoiding inconsistencies among different sea spray source functions under the microphysical framework (Details are given by *Zhang et al.* [2015b]). Here β_* represents the wave age, which is computed by the significant wave height; n and m are the Charnock relative parameters and set to be 0.42 and −1.03, respectively [*Donelan*, 1990]; ω is the correction parameter indicating the impact of sea spray on the logarithmic wind profile

$$\omega = \min\left(1, a_{cr}/\kappa u_*\right), \tag{19}$$

where a_{cr} represents a critical value of the terminal velocity of falling sea spray droplets, and is set to be 0.64 m/s based on the observations of Powell [*Makin*, 2005].

For low winds, the sea spray does not evidently affect the sea surface roughness. For high winds, the spray droplets over the ocean form a very stable and limiting saturation boundary layer, which restrains momentum transfer from the surface wind to the ocean (Figure 2). Therefore, spray droplets can influence the airflow dynamics at wind speeds exceeding 33 m/s [*Powell et al.*, 2003; *Jarosz et al.*, 2007)]. The drag coefficient calculated by equation (18) is in agreement with the "observed" drag coefficient [*Zhang et al.*, 2015b, Figure 2]. Hence, the sea surface aerodynamic roughness length z_0 (equation (18)) is used to calculate the drag coefficient and the total air-sea momentum flux. At the same time, the dynamic effects of sea spray are introduced by the new z_0 (equation (18)) to investigate the impact sea spray on the air-sea momentum exchange during the typhoon passage.

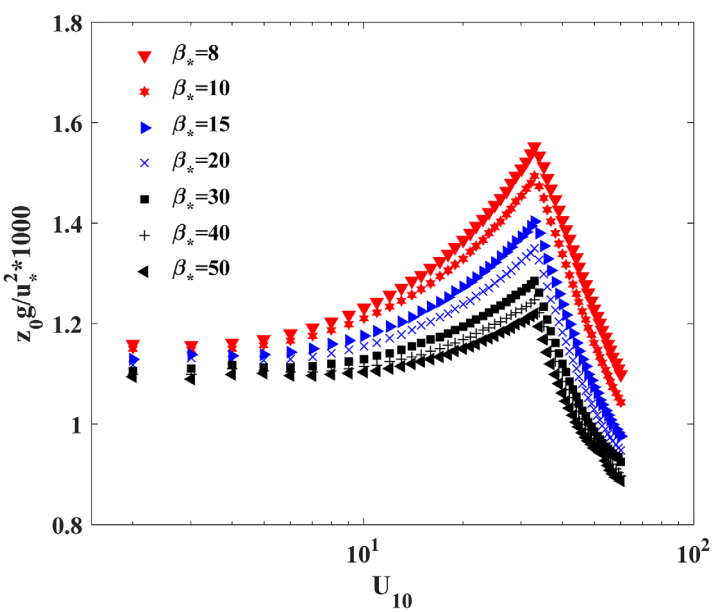

Figure 2. z_0g/u_*^2 versus sea surface wind for the different wave age condition (8, 10, 15, 20, 30, 40, and 50).

2.4. Combine Fluxes

The sea spray-induced and air-sea interfacial turbulent fluxes are combined as the air-sea total turbulent fluxes, which constitute the boundary conditions at

the lowest level of the COARE bulk model. But the total air-sea turbulent fluxes in the model cannot be simply added by both the sea spray induced fluxes and interfacial fluxes.

On the heat fluxes aspect, there are the complicated physical processes between the air-sea interface and the sea spray: (1) the existence of sea spray ultimately changes the average temperature and humidity profile in the sea spray evaporate layer; (2) it is impossible for all the sea spray droplets to come out on the top of the sea spray evaporation layer for sensible and latent heat exchange. Therefore, the total air-sea fluxes of sensible ($H_{S,T}$) and latent ($H_{L,T}$) heat fluxes are given by the complicated physical processes [*Andreas and DeCosmo*, 1999]

$$H_{L,T}=H_L+\alpha Q_l, \tag{20a}$$

$$H_{S,T}=H_S+\beta Q_s-(\alpha-\gamma)Q_l, \tag{20b}$$

where α, β, and γ are parameters, and obtained from the statistical fitting. In equation (20a), αQ_l is the sea spray-induced latent heat flux on the top of the spray evaporation layer. In equation (20b), however, $-\alpha Q_l$ is the atmospheric heat supply to evaporate the sea spray; βQ_s is the directly induced sensible heat flux by sea spray droplets in the cooling processes from the ocean surface temperature to the temperature for their returning to the sea surface; γQ_l is the added sensible heat flux to the spray evaporation layer due to the increase of the air-ocean temperature difference caused by the evaporation of sea spray. Based on data from the main experiment in the Humidity Exchange Over the Sea (HEXOS), the values of α, β, and γ are given by 3.3, 5.7, and 2.8, respectively [*Andreas*, 2003]. The sea spray induced by the net sensible ($Q_{S,sp}$) and latent heat fluxes ($Q_{L,sp}$) are estimated by

$$Q_{S,sp}=5.7Q_s-3.3Q_l+2.8Q_l, \tag{21a}$$

$$Q_{L,sp}=3.3Q_l. \tag{21b}$$

On the momentum fluxes aspect, the total air-sea momentum flux M_{tot} (including the dynamic effect of sea spray) is computed by the improved COARE version 2.6 bulk model, which introduces the parameterization of dynamic effect of sea spray equation (18) (sea surface dynamic roughness length including the effect of sea spray for the full wind speed conditions). In contrast, the interfacial air-sea momentum flux M_{int} (excluding the dynamic impact of sea spray) is calculated by the traditional Charnock relation equation (8) (the Charnock parameter is equal to 0.011). The sea spray induced air-sea momentum flux M_s is

$$M_s=M_{tot}-M_{\text{int}}. \tag{22}$$

3. Experiment Design

The POMgcs model is spun up for 5 years and then integrated for 5 years from January 1999 to December 2011. Typhoon Rammasun crosses the YES from 3 to 6 July 2002 (Figure 3). Four experiments are designed to investigate the influence of sea spray on the YES upper layer thermal structure during the passage of typhoon Rammasun, based on the POMgcs model, COARE air-sea turbulent model, and the parameterization of the sea spray: (1) the control run, (2) the dynamic effect of sea spray is included, (3) the thermal effect of sea spray is included, (4) both the thermal effect and the dynamic effect of sea spray are included. Detailed experimental setups are described in Table 1.

4. Results

4.1. Impact on the Air-Sea Turbulent Fluxes

Figures 4 and 5 show the latent and the sensible heat fluxes during the passage of Typhoon Rammasun in the YES, respectively. Figures 4a–4d and 5a–5d are the sea spray induced net sensible and latent heat fluxes. Figures 4e–4h and 5e–5h are the corresponding interfacial sensible and latent heat fluxes. The air-sea latent heat transfer is enhanced by the sea spray evaporation from the ocean to the atmosphere (Figures 4a–4d), while the sensible heat transfer is increased from the atmosphere to the ocean (Figures 5a–5d) owing to the complicated physical processes between the air-sea interface and the sea spray. Different from the interfacial latent and sensible heat fluxes, the sea spray induced net latent and sensible heat fluxes primarily locate around the eye-wall region of Typhoon Rammasun. Also, the maximum sea spray mediated

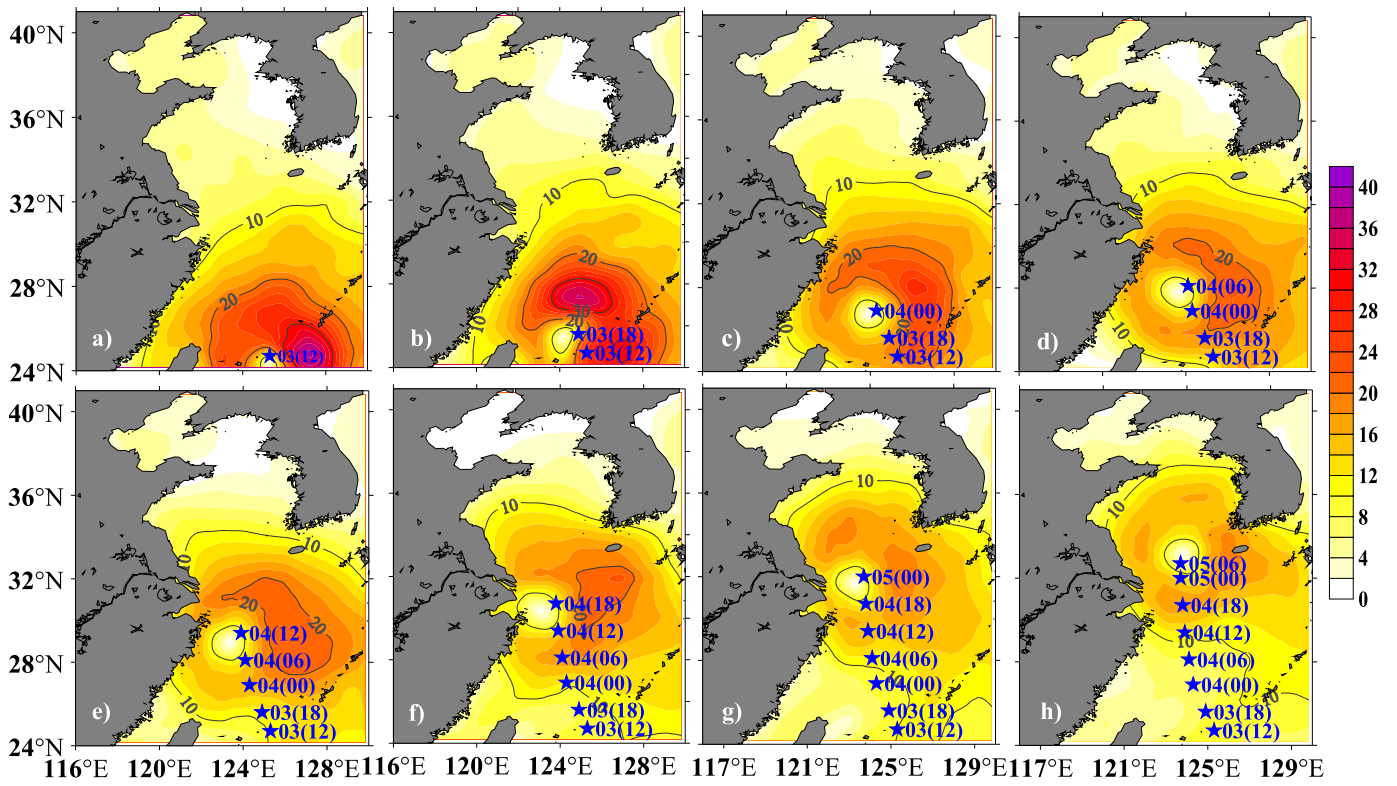

Figure 3. Sea surface wind speeds (m/s) at (a–h) 1200 UTC 3–0006 UTC 5 July 2002. Moving tracks of Rammasun are depicted with Pentacle.

net heat fluxes mostly lie on the right of the typhoon moving tracks (right bias), consistent with the distribution of the wind speed during Rammasun's passage (Figure 3). In addition, when Rammasun reaches the East China Sea at 1800 UTC, 3 July, the maximum sea spray-mediated net latent (sensible) heat flux is enhanced with up to 65 (−27) W/m^2, which is a 26% (13.5%) increase compared to the interfacial latent (sensible) heat flux (Figures 4b, 4f, 5b, and 5f). When Rammasun keeps up moving northward on 4 July, the typhoon-induced sea spray droplets still affect the air-sea heat fluxes with sea surface mean wind speed over 26 m/s. In a word, the sea spray enhances both the air-sea latent and sensible heat fluxes, especially for the latent heat fluxes. Although the sea spray mediated net sensible heat flux is negative, the ocean finally loses more heat by the effect of sea spray because the sea spray meditated net latent heat flux is larger than net sensible heat flux.

When the sea spray droplets eject into the air-sea interface, they accelerate almost immediately to the local wind speed. This process extracts momentum from the near-surface wind and therefore slows it [*Andreas and Emanuel*, 2001]. When sea spray droplets crash back into the sea surface, they transfer their momentum to the ocean [*Edson*, 1990]. In this process, the sea spray droplets finish the momentum transfer from the atmosphere to the ocean. To analyze how the sea spray droplets affect the structure of the air-sea momentum fluxes during Rammasun's passage over the YES, the sea spray induced momentum flux (Figures 6a–6d) and interfacial momentum flux (Figures 6e and 6h) are calculated. One can see from Figure 6 that the asymmetric interfacial momentum flux is well produced (Figures 6e–6f), and the air-sea momentum flux near the eye-wall region is significantly enhanced by considering the effect of sea spray (Figures 6a–6d).

Table 1. Experiment Setups

Experiment	Surface Momentum Fluxes	Surface Heat Fluxes
Exp_1	Interfacial momentum flux (M_{int}, no spray)	Interfacial heat fluxes ($H_L + H_S$, no spray)
Exp_2	Total momentum flux (M_{tot}, with spray)	Interfacial heat fluxes ($H_L + H_S$, no spray)
Exp_3	Interfacial momentum flux (M_{int}, no spray)	Total heat fluxes ($H_{L,T} + H_{S,T}$, with spray)
Exp_4	Total momentum flux (M_{tot}, with spray)	Total heat fluxes ($H_{L,T} + H_{S,T}$, with spray)

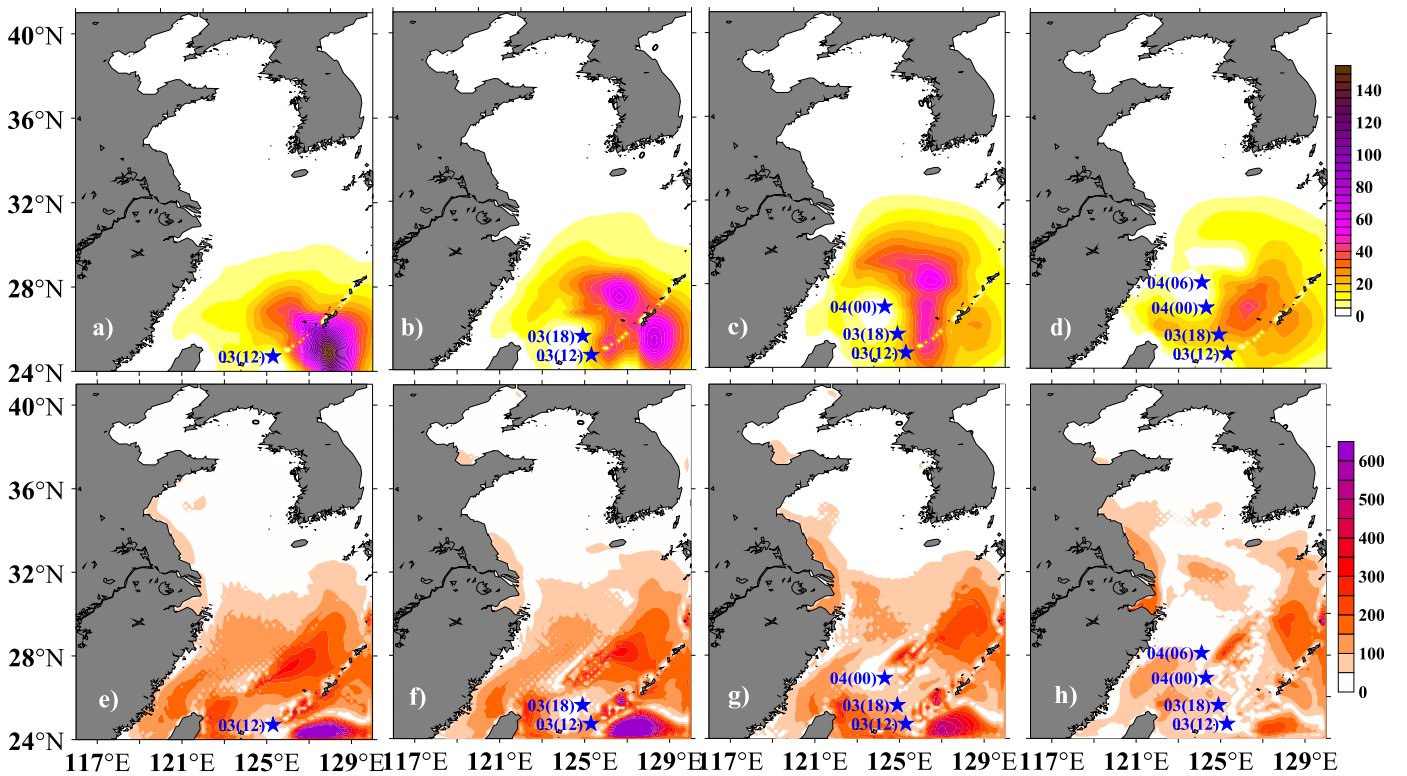

Figure 4. Sea spray induced net latent heat flux (W/m^2) at (a–d) 1200 UTC 3–0006 UTC 4 July 2002. Interfacial latent heat flux (W/m^2) at (e–h) 1200 UTC 3–0006 UTC 4 July 2002. Moving tracks of Rammasun are depicted with Pentacle.

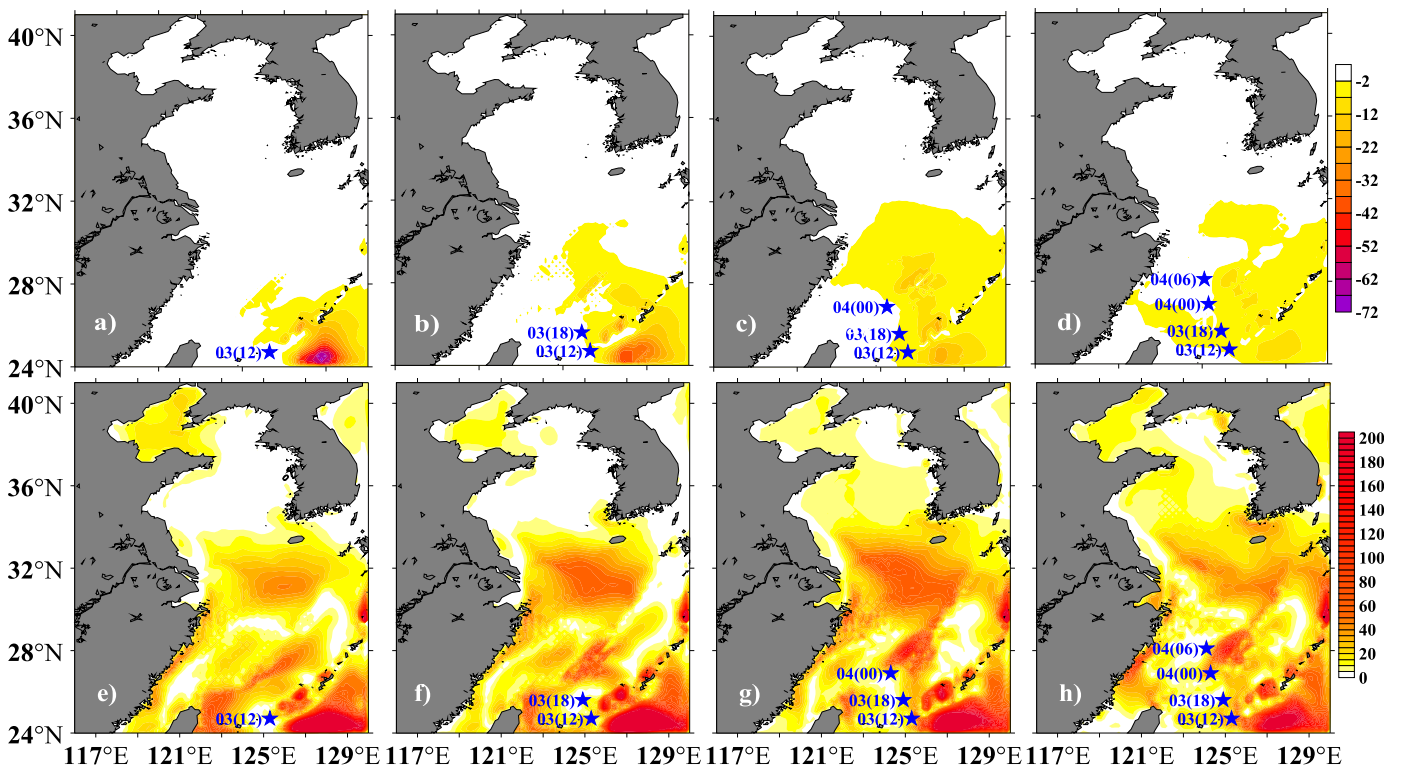

Figure 5. Same as Figure 4, but for sensible heat flux (W/m^2).

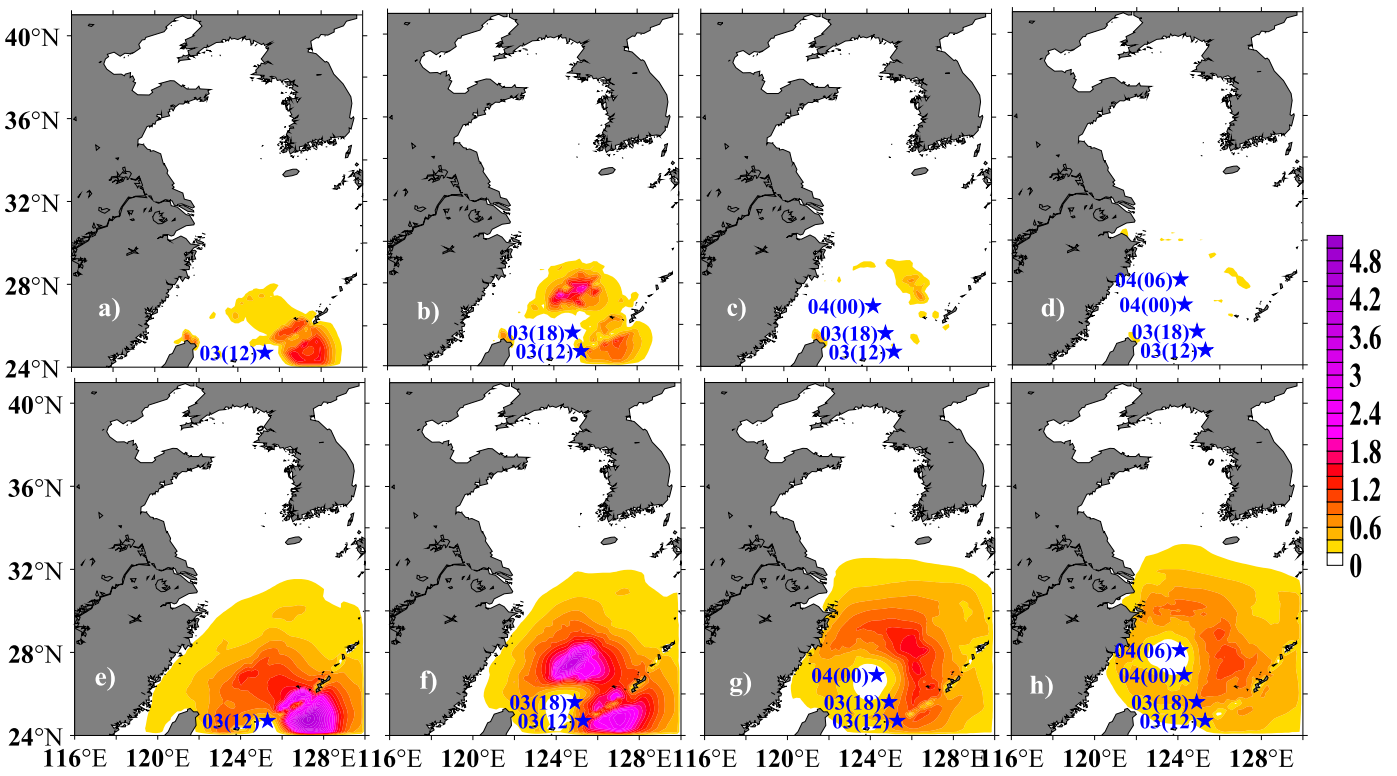

Figure 6. Same as Figure 4, but for momentum flux (N/m^2).

Also, the sea spray has the greatest contribution near the right of Rammasun moving tracks, consistent with the distribution of the biggest wind speed and significant wave height during Rammasun's passage (not shown). When Rammasun arrives in the East China Sea at 1800 UTC 3 July 2002, the maximum total air-sea momentum flux is enhanced by up to 1.9 N/m^2, which is an increment of about 43% compared with the interfacial momentum flux (Figures 6b and 6f).

4.2. Impact on the Sea Surface Temperature

The response of sea surface temperature (SST) to Rammasun is revealed by Satellite observations derived from AMSRE (Figure 7) and AVHRR (Figure 8). Rammasun formed in the northwest Pacific on 29 June 2002, while it was upgraded to a super typhoon and entered the study area. Before Rammasun arrived in the region, the area south of 30°N is generally occupied by the warm water of 27°C, and the SST between 30°N and 36°N basically exceeded 20°C (Figures 7a and 8a). When Rammasun arrived in the East China Sea on 4 July, there was a broad area of low SST around the right-hand side of Rammasun, especially for the

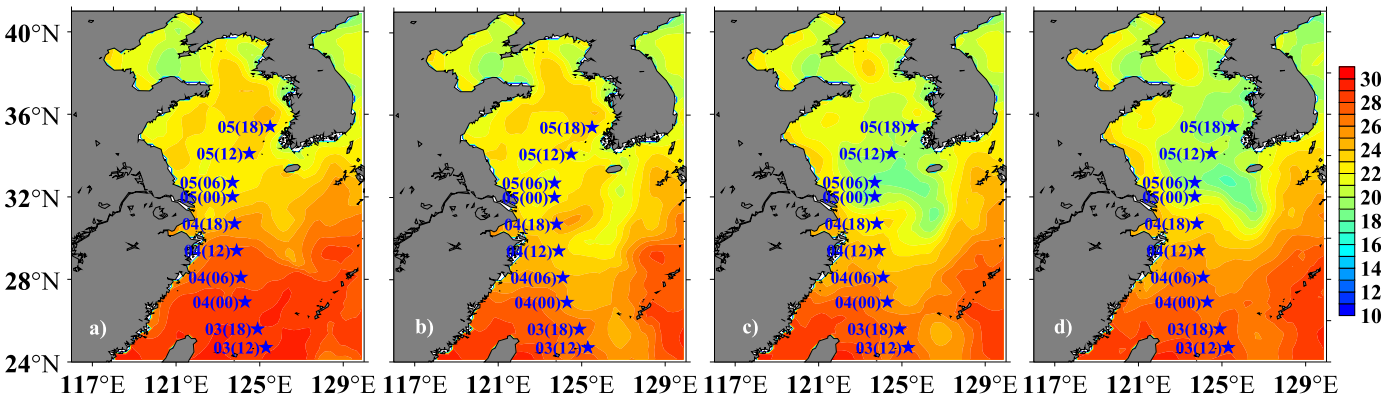

Figure 7. The AMSRE SST images on (a–d) 3–6 July 2002. Moving tracks of Rammasun are depicted with Pentacle.

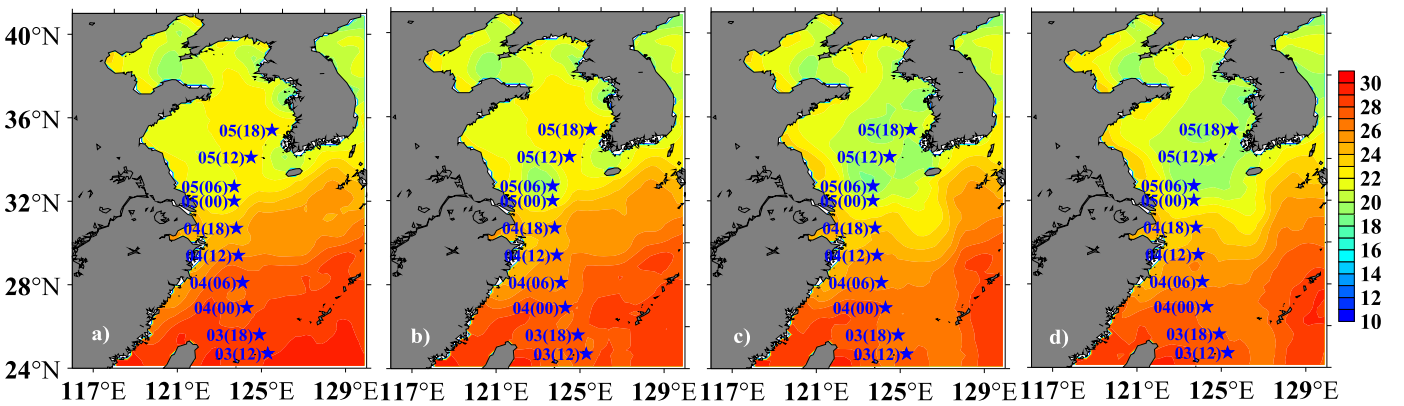

Figure 8. Same as Figure 7, but for SST from AVHRR.

observations from AMSRE. The maximum cooling of SST was on the right side of Rammasun from 24.25°C on 3 July to 21.5°C on 4 July (Figure 7b). Subsequently, Rammasun moved northeast to reach the Yellow Sea on 5 July, and the broad area of low SST was found around the Rammasun (Figures 7c and 8c). The SST on the right of Rammasun was greatly decreased from 22.5°C on 4 July to 18.25°C on 5 July from the AMSRE satellite (Figure 7c). In addition, the SST around the Rammasun declined from 22.5 to 20°C, shown from the AVHRR satellite observation (Figure 8c). Rammasun landed on 6 July, while the right-side area of Rammasun still remained the low temperature water.

Model-simulated daily SST derived from Test 1 (without the effect of sea spray, Figure 9) and Test 4 (with the effect of sea spray, Figure 10) are compared with the satellite observations. On 4 July, the areas of low temperature on the right of Rammasun are also shown in the two tests. During the prety-phoon period, the simulated SST dropped to 23.25°C on 4 July in Test 1 (Figure 11c), and to 21.75°C (Figure 11d) in Test 4 (considering the effect of sea spray), which is closer to the observations from the AMSRE (Figure 11a). When Rammasun reaches the Yellow Sea on 5 July, the area around the Rammasun revealed low temperature region (Figures 9c and 10c). When the effect of sea spray is considered, the low temperature area of 20°C around Rammasun is bigger than Test 1, closer to the satellite observations of AVHRR (Figure 12).

Hence, the comparison of the surface cooling derived from the simulated results with satellite observations indicates that the sea spray droplets have a significant impact on improving the response of SST to Rammasun's passage. It is worth noting that the locations of the most strong SST cooling simulated by POMgcs does not completely agree with the satellite observation owing to somewhat difference between the CCMP wind field and the actual typhoon field (such as the position of typhoon eye, the maximum wind speed of typhoon, etc.).

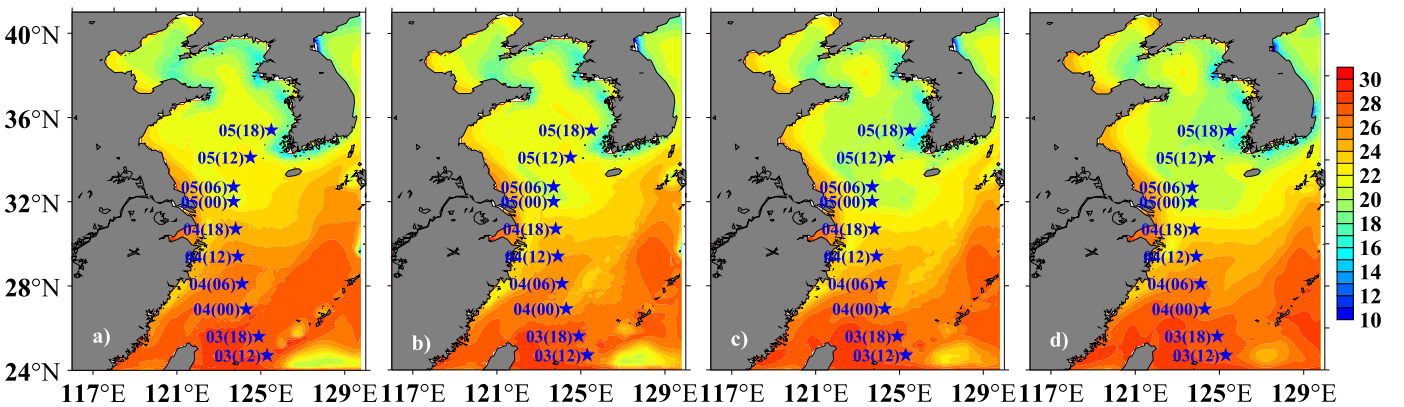

Figure 9. Same as Figure 7, but for SST from Test 1.

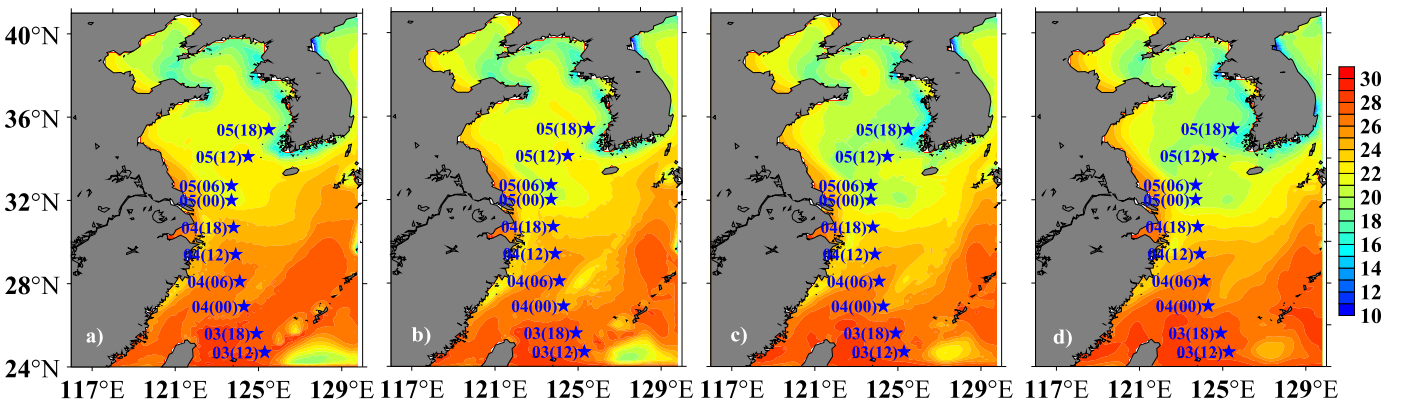

Figure 10. Same as Figure 7, but for SST from Test 4.

4.3. Impact on the Upper Ocean Thermal Structure

With the location of Rammasun eye as a reference at 0600 UTC 4 July, the sea temperature section from the sea surface to 100 m depth along 28.1°N is investigated (Figure 13). Test 1 is used to analyze the change of the upper ocean temperature during Rammasun's passage. Before the edge of Rammasun passed the section of 28.1°N, the ocean temperature is uniformly distributed in the shallow of 50 m depth. When Rammasun swept this ocean section, the isotherms bend downward with the thermocline deepening (Figure 13). Associated with the thermocline down welling, the cooling near the sea surface is accompanied by the warming in the subsurface [*Price*, 1981; *D'Asaro et al*., 2007, 2014]. The sea surface and near-surface cooling is primarily caused by the vertical mixing associated with strong typhoon winds. The ocean heat is transported from the sea surface to the ocean subsurface by the typhoon-induced vertical mixing, which results in the sea surface or near-surface cooling and ocean subsurface warming. This phenomenon is named as the "heat pump" of typhoon passage [*Emanuel*, 1986; *Chen et al*., 2013].

To further analyze the effect of sea spray on the response of upper ocean to the typhoon, the latitude-depth section of the upper ocean temperature along 28.1°N is shown in Figure 14, which is the difference between the posttyphoon upper ocean temperature and the pretyphoon one from Tests 1 to 4 (Figure 14). With Rammasun passing the section of 28.1°N, the cooling occurs in the upper ocean 14 m (the maximum is 3.35°C/d), while the warming takes place in the depth of 14–60 m (Figure 14a). Therefore, the process of the "heat pump" dominates as Rammasun passing the vertical section of 28.1°N. Considering the influence of sea spray induced momentum flux, the surface cooling, and the subsurface warming are evidently enhanced. The depth of the subsurface warming deepens to 74 m, and the maximum warming reaches 3.75°C at the depth of 46 m associated with the maximal curve of isotherm (Figure 14b). Unlike the effect of sea spray induced momentum flux, the sea spray induced net heat fluxes (sea spray induced net latent heat fluxes adds sea spray induced net sensible heat fluxes) slightly affects the process of "heat pump" (Figure

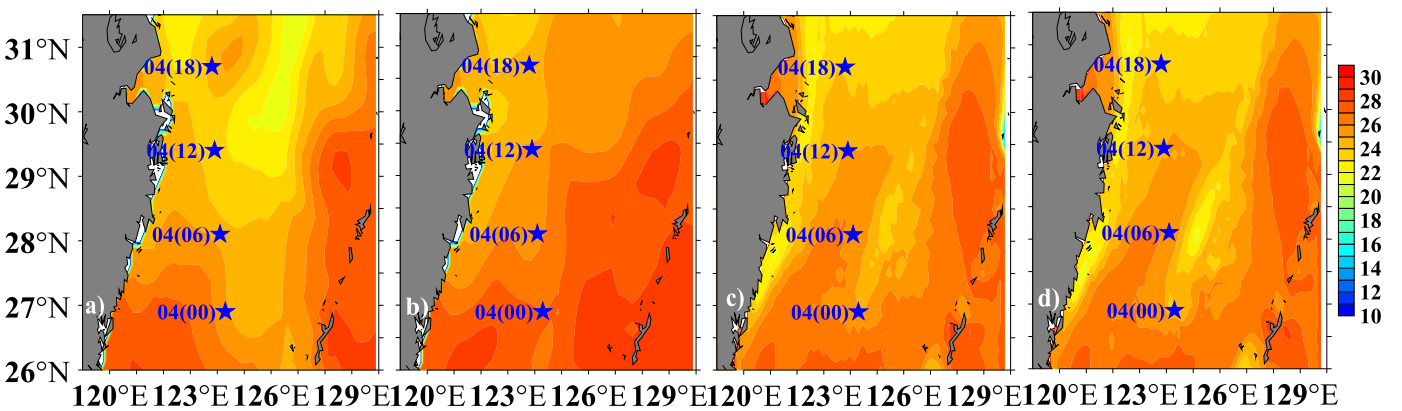

Figure 11. Daily averaged SST from (a) AMSRE; (b) AVHRR; (c) Test 1; (d) Test 4. Pentacle indicate the center location of Rammasun on 4 July (every 6 h).

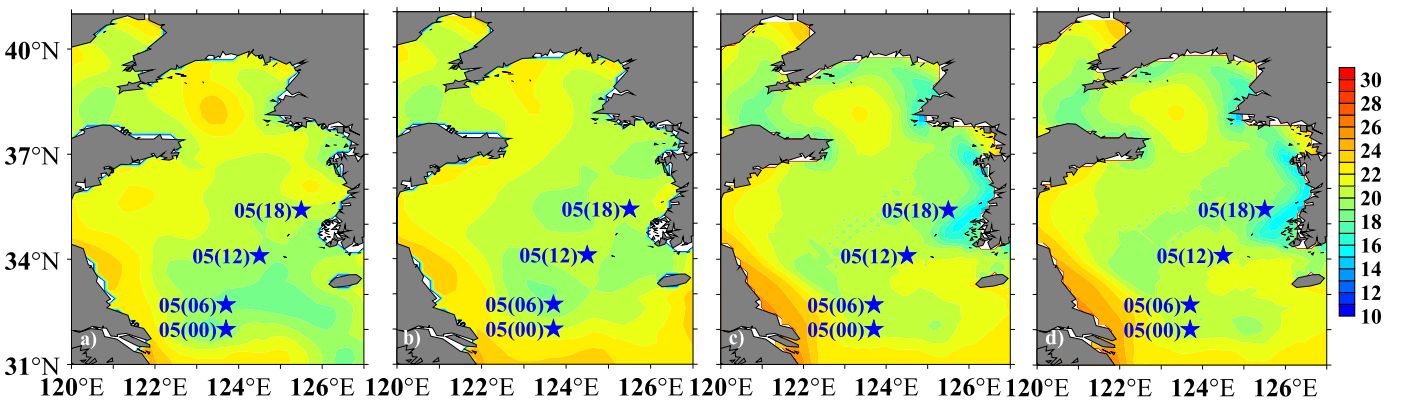

Figure 12. Daily averaged SST from (a) AMSRE; (b) AVHRR; (c) Test 1; (d) Test 4. Pentacle indicates the center location of Rammasun on 5 July (every 6 h).

14c). When the effect of sea spray induced heat and momentum fluxes is considered, the near-surface cooling and the subsurface warming are more enhanced. The depth of warming increases to 77 m. The maximum warming at 46 m reaches 5.68°C (Figure 14d). Thus, the ocean surface cooling and the mixed layer deepening reflect the dynamic and thermal responses of the upper layer to the typhoon forcing, and the influence of sea spray enhances the response of upper layer during Rammasun's passage.

In addition, the vertical section of 26.9°N is also selected to analyze the effect of sea spray on the upper ocean temperature response. The evolution of the upper ocean temperature between the pretyphoon and posttyphoon is shown in Figure 15. Comparing to the pretyphoon temperature section, all the isotherms rise under the Rammasun center along 26.9°N from the sea surface to the 100 m depth. The mixed layer temperature becomes colder, while the thermocline is evidently uplifted on 4 July in the posttyphoon period. The rise of the thermocline during the typhoon passage is produced by the cyclonic wind stress, which induces the strong cooling in the upper ocean without causing subsurface warming [*Park et al.*, 2011]. This phenomenon is called "cold suction" [*Chen et al.*, 2013]. The passage of the "cold suction" is also found from the Modular Ocean Assimilation System (MODAS) [*Fox et al.*, 2002], which is improved to generate three-dimensional (3-D) ocean temperature and salinity fields based on sea surface observations [*Wang et al.*, 2012] during the typhoon passage (Figure 16). Figure 16 shows that the isotherms from 0 to 100 m depth are lifted along 26.9°N, especially for the right side of the typhoon center.

Figure 17 shows the upper ocean temperature difference along 26.9°N between the pretyphoons and posttyphoons. When Rammasun passes the section, the sea temperature from 0 to 100 m depth is evidently decreased. The maximum cooling from the sea surface to 20 m depth, 1.75°C, is located at the underwater location of the Rammasun center, but the maximum cooling on the depth of 40 m is 2.0°C, which located at the underwater right side of the Rammasun center (Figure 17a). Thus, the process of "cold suction"

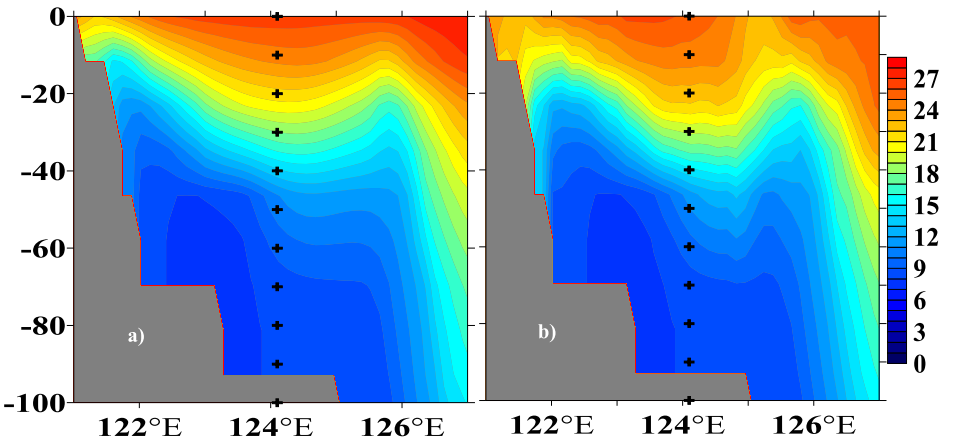

Figure 13. Ocean temperature (°C) from Test 1 in a vertical-zonal section along 28.1°N at (a) 0600 UTC 3 and 4 (b) July 2002.

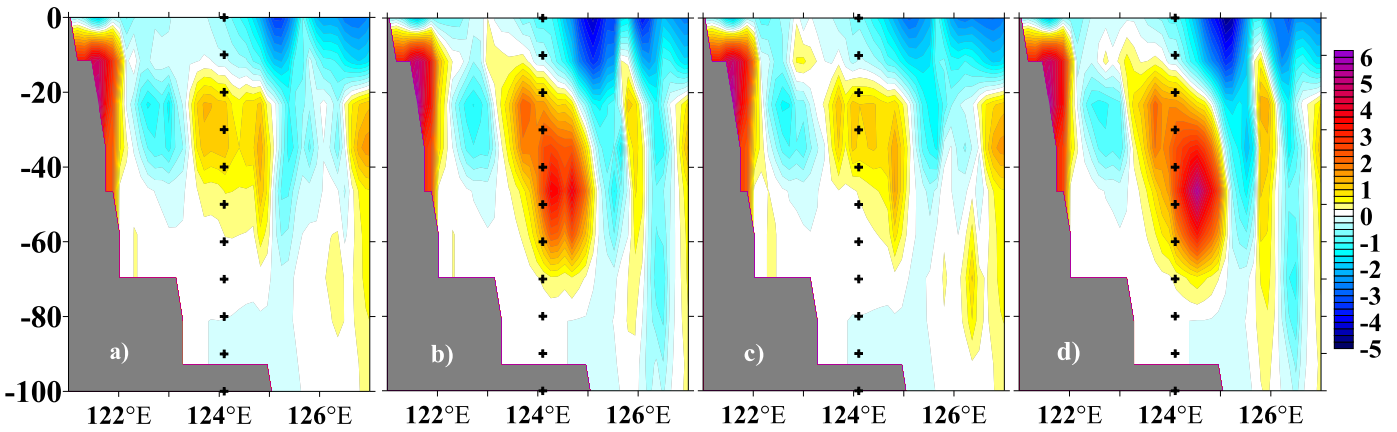

Figure 14. Ocean temperature difference (temperature at 0600 UTC 4 July 2002 minus 0000 UTC 4 July 2002) along 28.1°N from (a–d) Tests 1–4.

dominates as Rammasun passes the vertical section of 26.9°N. In the meanwhile, the effect of sea spray evidently enhances the process of the "cold suction" during the typhoon passage. Considering the influence of sea spray induced momentum flux, the maximum cooling at the depth of 20 m (40 m) increases to 2.0°C (2.25°C) with the increasing width of cooling area (Figure 17b). Unlike the effect of sea spray induced momentum flux, sea spray induced net heat fluxes slightly affect the process of "cold suction" (Figure 17c). Also, when the sea spray induced momentum and net heat fluxes are considered together, the process of the "cold suction" is further reinforced. The depth of the near-surface cooling increases to 30 m; and the maximum cooling at 40 m depth enhances to 2.5°C, which is 0.5°C colder than that of Test 1 (Figure 17d). Figure 18 compares the daily change of sea temperature along 26.9°N section with (Test 4) and without (Test 1) the influences of sea spray. The "cold suction" passage is revealed by the Test 4 and the Test 1, while the intensity of "cold suction" with sea spray is stronger with the sea spray effect (Test 4) than without the sea spray effect (Test 1), i.e., the 0.75°C isotherm is deepen from 75 m in the Test 1 to 95 m in the Test 4, which is closer to the MODAS data during Rammasun's passage.

4.4. Impact on Vertical Diffusion and Advection

In the ocean heat equation, the local time rate of change of temperature is caused by vertical diffusion, advection, and horizontal diffusion. Each term is calculated using four experimental data (Tests 1–4), as shown in Figures 19–21. Since the horizontal diffusion is not sensitive among the four tests (Figure 21), it is not analyzed. Without the effect of sea spray (Test 1), the vertical diffusion cools the temperature from the sea surface to 36 m depth below the center of Rammasun, while the maximum of the cooling rate is 0.75°C/d in the mixed layer. Also, the vertical diffusion warms the subsurface temperature in the 40–70 m depth below the right side of Rammasun center (Figure 19a). The advection term (including the horizontal advection and the vertical convection), however, warms the ocean from the sea surface to 50 m depth,

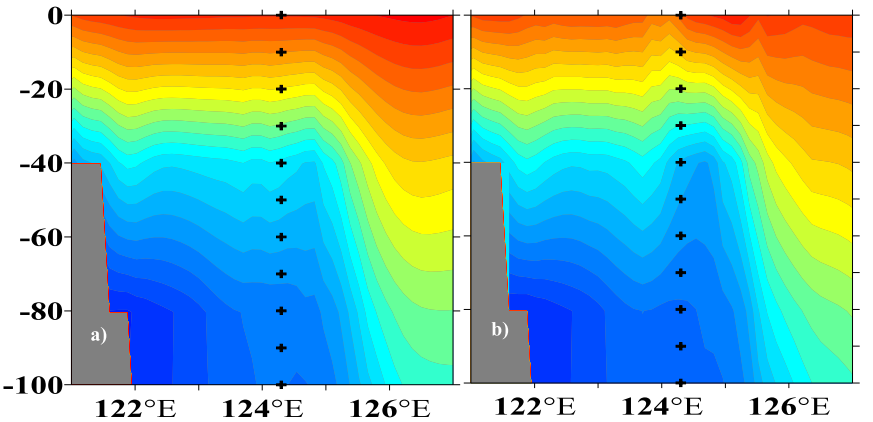

Figure 15. Ocean temperature (°C) from Test 1 in a vertical-zonal section along 26.9°N at (a) 0000 UTC 3 and 4 (b) July 2002.

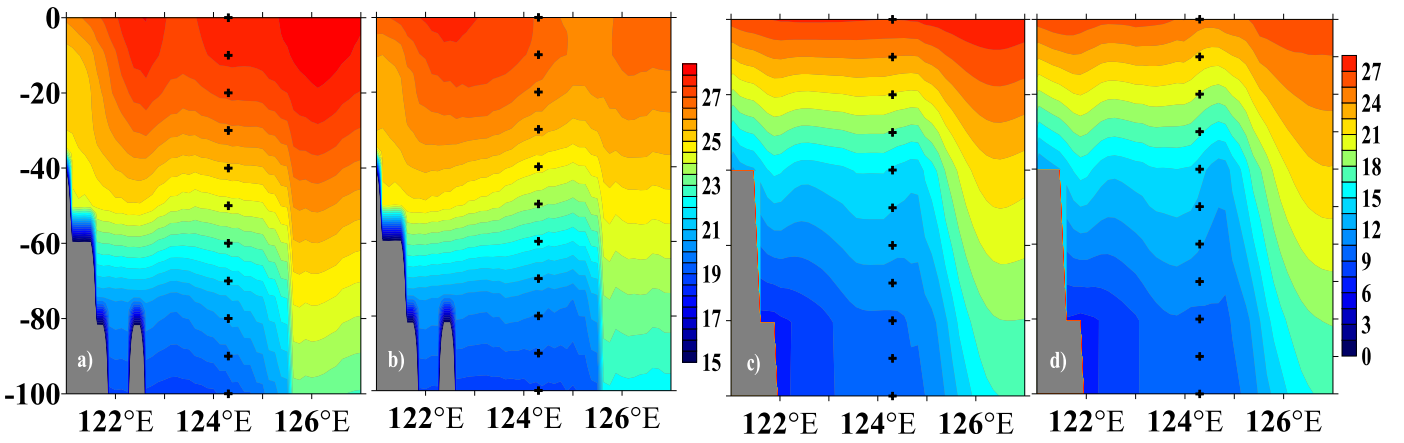

Figure 16. (a and c) Ocean temperature from MODAS and Test 1 in a vertical-zonal section along 26.9°N on 2 July 2002; (b and d) Ocean temperature derived MODAS and Test 1 on July 5 2002.

while the region of the maximal warming rate (1.75°C/d) is located from 22 to 32 m underwater below the Rammasun center (Figure 20a). This implies that the sea surface and near-surface cooling is caused primarily by the vertical diffusion, and the subsurface warming is modulated by the advection. In addition, the vertical diffusion also induces warming in the depths of 40–70 m. In other words, both the vertical diffusion and advection contribute to the sea surface or near-surface cooling and ocean subsurface warming, corresponding with the "heat pump" phenomenon in the 28.1°N section during the Rammasun's passage. Under the influence of the sea spray induced momentum flux (Test 2), both the vertical diffusion and advection are significantly enhanced. The cooling rate caused by the vertical diffusion in the upper 20 m depth is enhanced to 1.0°C/d, and its warming (2.5°C/d) is expanded to 40–70 m depth below Rammasun center (Figure 19b). At the same time, the ocean warming induced by advection extends to 50 m depth, with a maximum of 3°C/d in 25–30 m depths (Figure 20b). Different from the momentum flux, the sea spray induced net heat fluxes mainly affect the vertical diffusion in the near-surface (Test 3), the cooling rate of the vertical diffusion is added up to 1°C/d near the sea surface below the typhoon center (Figure 19c). However, when the effect of the sea spray on momentum and net heat flux is considered (Test 4), the warming induced by the vertical diffusion and advection is further enhanced. The warming rate caused by the vertical diffusion in 30–70 m depths reaches 3.5°C/d below the right side of Rammasun center (Figure 19d). The warming depth caused by the advection is extended to 55 m depth below the right side of Rammasun center (Figure 20d).

Similarly, contribution of vertical diffusion and advection to the upper ocean temperature in the 26.9°N section during the Rammasun's passage is investigated with and without the effect of sea spray. The vertical diffusion in Test 1 (without the effect of sea spray) causes the cooling in the upper 10 m below the typhoon center region, with a maximum cooling rate of 4°C/d at the sea surface (Figure 22a). The cooling at the

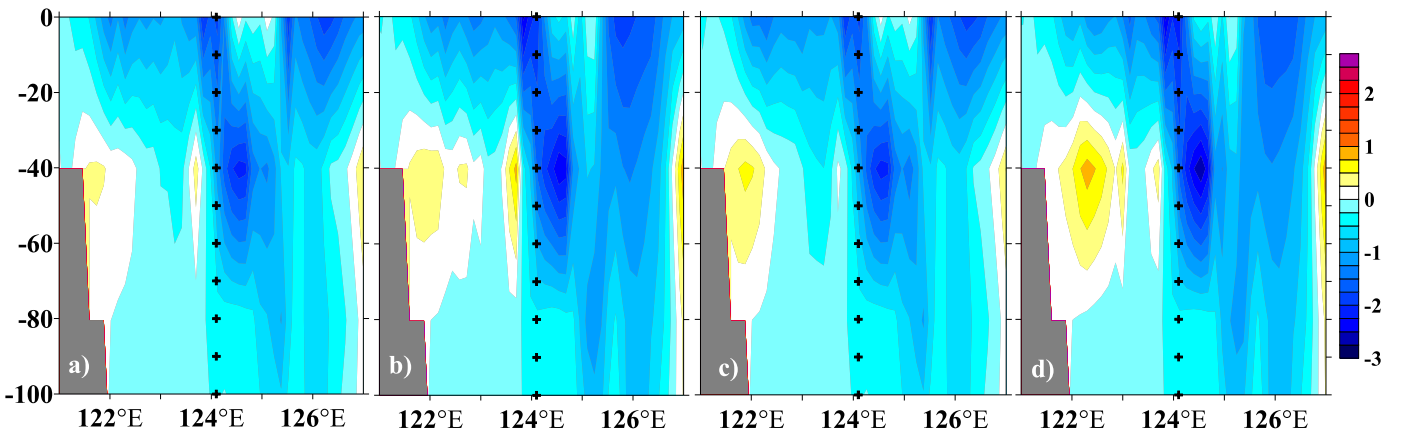

Figure 17. Ocean temperature difference (temperature at 0000 UTC 4 July 2002 minus 0000 UTC 3 July 2002) along 26.9°N from (a–d) Test 1–4.

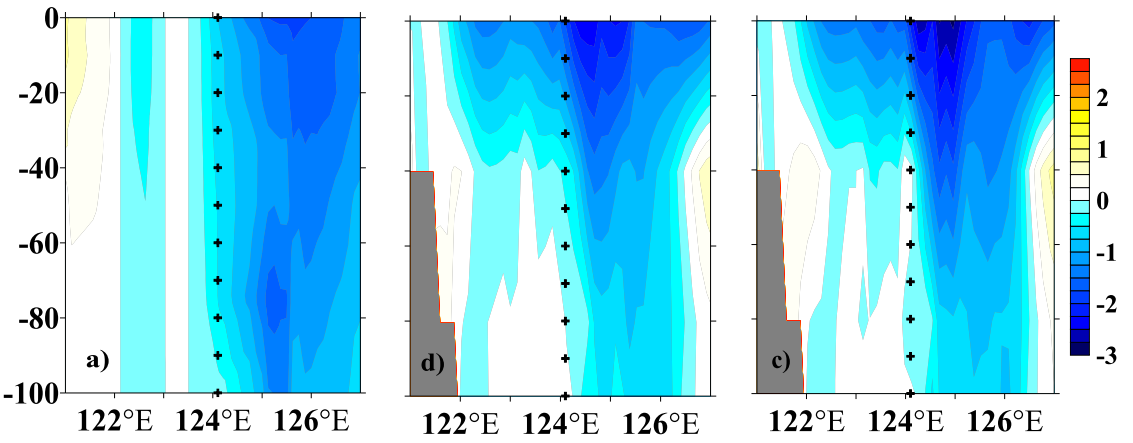

Figure 18. Ocean temperature different (temperature on 5 July 2002 minus 2 July 2002) along 26.9°N derived from (a) MODAS, (b) Test 1, and (c) Test 4.

depth from 10 to 100 m is induced by the advection, with a maximum cooling rate of 5°C/d at the depth from 20 to 28 m (Figure 23a). When Rammasun passes the vertical section of 26.9°N, the cooling in the upper (lower) 10 m is mainly dominated by the vertical diffusion (the advection). In other words, the advection transfers the subsurface cold water into the upper ocean layer, which raises the ocean thermocline. The colder water in the lower layer and warmer water in the upper layer are vertically mixed by the vertical diffusion. Affected by both the vertical mixing and advection entrainment, the enhanced cooling happens in the upper 100 m depth below the Rammasun center region ("cold suction"). Considering the effect of sea spray induced momentum flux (Test 2), the affected depth and intensity of the vertical diffusion and advection are significantly enhanced. The maximum cooling rate increases to 5.9°C/d near the sea surface due to the vertical diffusion with the sea spray mediated momentum flux (Figure 22b); and to 7.8°C/d in the depth from 20 to 28 m due to the advection (Figure 23b). Taking into account the effect of sea spray on the net heat fluxes (Test 3), the cooling rate due to the vertical diffusion is added up to 4.7°C/d near the surface (Figure 22c), while due to the advection is almost unchanged. However, when the effect of sea spray heat and momentum fluxes is considered (Test 4), the cooling rate is further enhanced. The subsurface cooling rate related to the vertical diffusion is up to 6.1°C/d in the upper 14 m (Figure 22d). The cooling depth of the advection is extended to 46 m depth below the right side of Rammasun center (Figure 23d).

From the above analysis, the effect of the sea spray on momentum flux significantly enhances the vertical diffusion and advection of the temperature field. Different with the effect of sea spray momentum flux, the net heat flux mainly strengthens the vertical diffusion. Although the effect of the sea spray caused net heat fluxes is smaller than that of the sea spray caused momentum flux, the combined effects of momentum

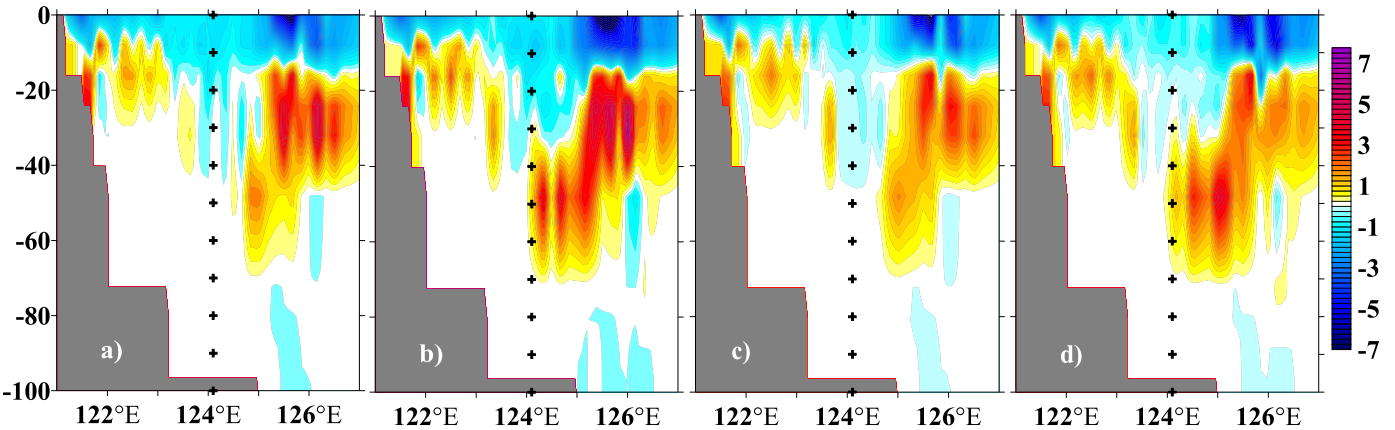

Figure 19. The vertical diffusion of ocean temperature (°C/d) corresponding with Figure 14, from (a–d) Tests 1–4.

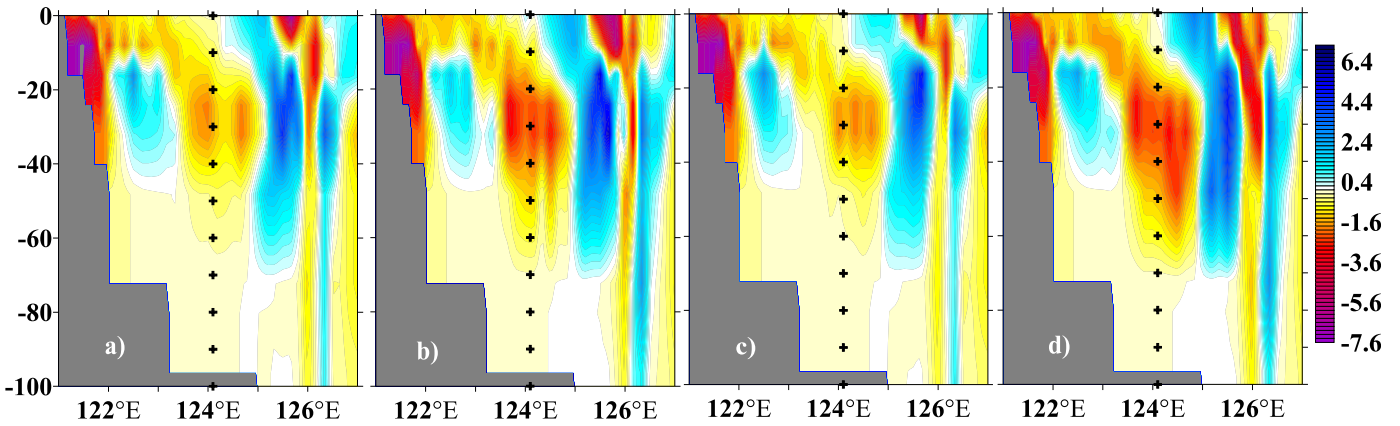

Figure 20. Same as Figure 19, but for the advection of ocean temperature.

and heat induced by the sea spray are stronger than the individual one since there is interaction between them.

5. Conclusions

The 3Dvar POMgcs ocean model is used to investigate the effect of sea spray on the upper ocean response to Rammasun in the YES from 3 to 6 July 2002. The effects of sea spray caused heat and momentum fluxes are introduced by two physical processes. First, the sea spray induced heat fluxes are introduced with improved Fairall's sea spray heat fluxes algorithm, which includes the new whitecap areal fraction and the feedback mechanism between the air-sea interface and the sea spray. Second, the sea spray affected momentum flux is considered through the improved COARE version 2.6 bulk model, in which the spray-affected sea surface dynamic roughness length is used for the full wind speed condition. Third, the sea spray induced momentum and heat fluxes are completely considered to analyze the impact of sea spray on the sea temperature during the passage of Rammasun.

The sea spray induced turbulent fluxes are primarily located around the eye-wall region of Typhoon Rammasun. The maximum effects mostly lie on the right of the typhoon moving tracks, consistent with the distribution of wind speed during Rammasun's passage (right-side bias). When Rammasun reaches the Yellow sea, the maximum sea spray net latent (sensible) heat flux is enhanced up to 65 (−27) W/m^2, which is a 26% (13.5%) increase compared to the interfacial latent (sensible) heat flux. The maximum total air-sea momentum flux is enhanced up to 1.9 N/m^2, which is 43% increase compared to the interfacial momentum flux.

The sea spray induced momentum flux significantly enhances the vertical diffusion and the advection for the sea temperature, while sea spray induced net heat fluxes mainly strengthens the vertical diffusion.

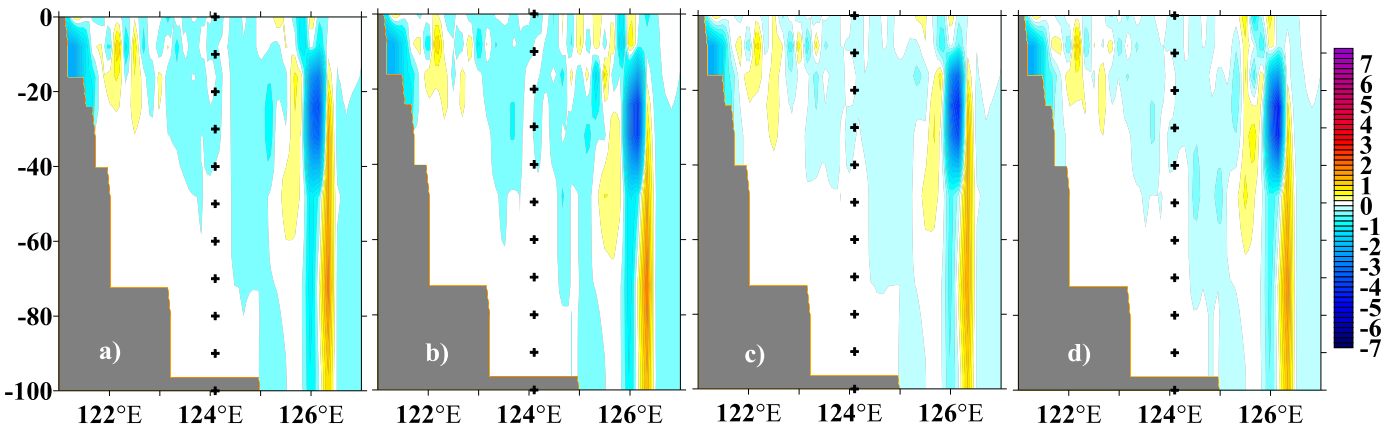

Figure 21. Same as Figure 19, but for the horizontal diffusion of ocean temperature.

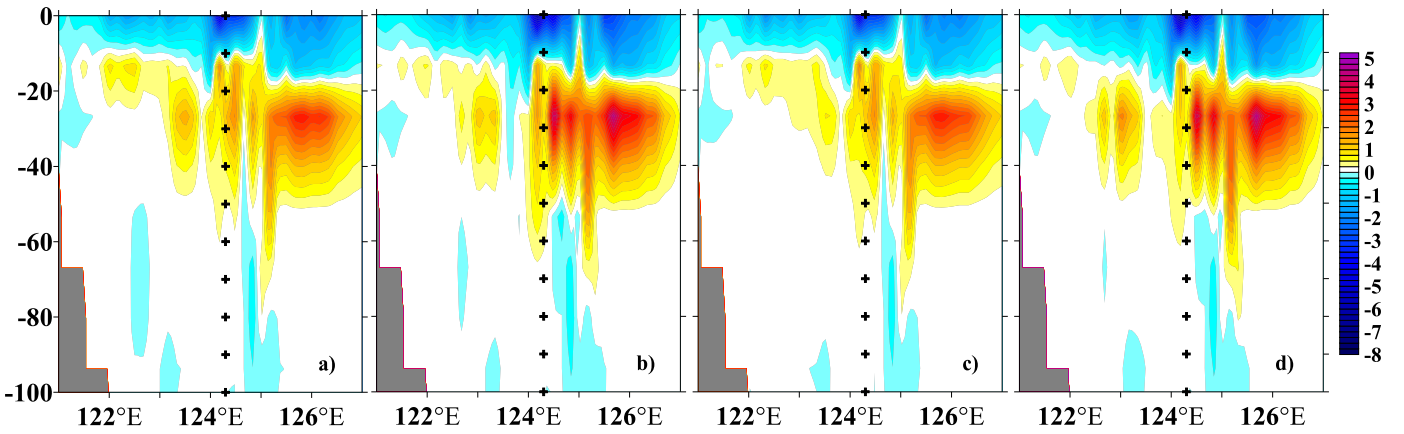

Figure 22. The vertical diffusion of ocean temperature (°C/d) corresponding with Figure 17, from (a–d) Tests 1–4.

Although the effect of the sea spray net heat fluxes is smaller than the sea spray induced momentum fluxes, there is a positive feedback process between the two to further affect the heat budget of the upper ocean. Hence, the combined effects of heat and momentum fluxes induced by the sea spray are stronger than the individual one.

In addition, the inclusion of sea spray effects can significantly enhance the intensity of the "cold suction" and "heat pump" during the Rammasun's passage. In the process of the "cold suction", the sea spray enhances the cooling at 60 m depth under the typhoon center position. The maximum sea surface cooling induced by the sea spray is enhanced by 0.5°C in the right side of the typhoon track, which consists with the satellite observations. Hence, sea spray acts as an additional source of the air-sea turbulent fluxes and can improve the upper ocean thermal response during the Rammasun's passage.

In addition, for a complicate air-sea relative reaction typhoon, the effects of wave also play a key role in affecting air-sea turbulent fluxes [*Reichl et al.*, 2014], ocean state and sea spray generation [*Zhang and William*, 2006]. When sea spray returns to water, sea spray extinguishes short waves to reduce the drag induced by wave [*Andreas*, 2004; *Makin and Kudryavtsev*, 1999]. To illustrate clearly the effects of sea spray, this study only considers the thermal and dynamic effects of sea spray on the mid-latitude upper ocean during a typhoon passage. However, some discrepancies still exist between the observation and the simulation due to the use of ocean model only. First, wave drag may compete or mitigate some of the effects of sea spray [*Liu et al.*, 2012], thus we will use a wave model to provide the source of the sea spray [*Zhang et al.*, 2006; *Zhang and Perrie*, 2008], and supply more proper relation between sea surface wind and wave for the passage of typhoons [*Donelan et al.*, 1985]. Second, the air-sea coupled model should be used in future to understand the feedback processes between sea spray and air-sea interface.

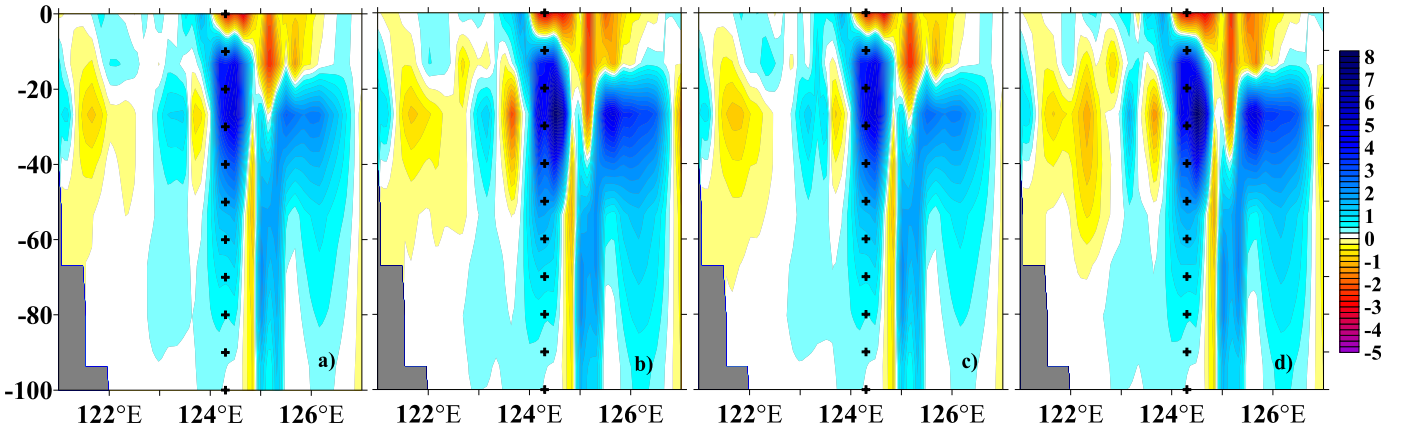

Figure 23. Same as Figure 22, but for the advection of ocean temperature.

Acknowledgments
Supported by National Key Research and Development Program of China (2016YFC1401800), National Programme on Global Change and Air-Sea Interaction of China (GASI-IPOVAI-04), National Basic Research Program of China (2013CB430304), and National Natural Science Foundation of China (41376013, 41606039, 41541041, and 41506039). The authors are particularly grateful to D. Karnauskas and two anonymous reviewers for their careful reviews and valuable comments, which led to substantial improvement of this manuscript. The data and code (in MATLAB and FORTRAN formats) used in this paper can be obtained from the first author (zhanglianxinde@163.com).

References

Andreas, E., and L. Mahrt (2016), On the prospects for observing spray-mediated air-sea transfer in wind-water tunnels, *J. Atmos. Sci.*, *73*, 185–198.
Andreas, E. L. (1989), Thermal and size evolution of sea spray droplets, *CRREL Rep. 89–11*, 37 pp., U.S. Army Cold Reg. Res. and Eng. Lab., Hanover, N. H.
Andreas, E. L. (1990), Time constants for the evolution of sea spray droplets, *Tellus, Ser. B*, *42*, 481–497.
Andreas, E. L. (1992), Sea spray and the turbulent air-sea heat fluxes. *J. Geophys. Res.*, *97*, 11,429–11,441.
Andreas, E. L. (1994), Reply, *J. Geophys. Res.*, *99*, 14,345–14,350.
Andreas E. L. (1998), A new sea spray generation function for wind speeds up to 32 ms^{-1}, *J. Phys. Oceanogr.*, *28*(11), 2175–2184.
Andreas, E. L. (2003), An algorithm to predict the turbulent air-sea fluxes in high-wind, spray conditions. Preprints, 12th Conference on Interaction of the Sea and Atmosphere, Long Beach, CD-ROM, 3.4, Am. Meteorol. Soc., San Diego, Calif.
Andreas, E. L. (2004), Spray stress revised, *J. Phys. Oceanogr.*, *34*, 1429–1440.
Andreas, E. L. (2010), Spray-mediated enthalpy flux to the atmosphere and salt flux to the ocean in high winds, *J. Phys. Oceanogr.*, *40*(3), 608–619.
Andreas, E. L., and J. DeCosmo (1999), Sea spray production and influence on air-sea heat and moisture fluxes over the open ocean, in *Air-Sea Exchange: Physics, Chemistry and Dynamics*, edited by G. L. Geernaert, pp. 327–362, Kluwer.
Andreas, E. L., and K. A. Emanuel (2001), Effects of sea spray on tropical cyclone intensity, *J. Atmos. Sci.*, *58*, 3741–3751, doi:10.1175/1520-0469(2001)058,3741:EOSSOT.2.0.CO;2.
Andreas, E. L., P. O. G. Persson, and J. E. Hare (2008), A bulk turbulent air-sea flux algorithm for high-wind spray conditions, *J. Phys. Oceanogr.*, *38*(7), 1581–1596.
Bao, J. W., J. M. Wilczak, J. K. Choi, and L. H. Kantha (2000), Numerical simulations of air-sea interaction under high wind conditions using a couple model: A study of hurricane development, *Mon. Weather Rev.*, *128*, 2190–2210.
Blumberg, A. F., and G. L. Mellor (1987), A description of a three-dimensional coastal ocean circulation model, in *Three-Dimensional Coastal Ocean Models*, pp. 1–16, AGU, Washington, D. C.
Charnock, H. (1955), Wind stress on a water surface, *Q. J. R. Meteorol. Soc.*, *81*, 639–640.
Chen, D. K., X. T. Lei, W. Wang, G. H. Wang, G. J. Han, and L. Zhou (2013), Upper ocean response and feedback mechanisms to typhoon [in Chinese], *Adv. Earth Sci.*, *28*(10), 1077–1086.
Chu, P. C., and K. F. Cheng (2007), Effect of wave boundary layer on the sea-to-air dimethylsulfide transfer velocity during typhoon passage, *J. Mar. Syst.*, *66*, 122–129.
Chu, P. C., J. M. Veneziano, C. W. Fan, M. J. Carron, and W. T. Liu (2000), Response of the South China Sea to tropical cyclone Ernie 1996, *J. Geophys. Res.*, *105*, 13,991–14,009.
D'Asaro, E. A., T. B. Sanford, P. P. Niiler, and E. J. Terrill (2007), Cold wake of Hurricane Frances, *Geophys. Res. Lett.*, *34*, L15609, doi:10.1029/2007GL030160.
D'Asaro, E. A., et al. (2014), Impact of typhoons on the ocean in the Pacific: ITOP, *Bull. Am. Meteorol. Soc.*, *95*, 1405–1418, doi:10.1175/BAMS-D-12-00104.1.
Donelan, M. A. (1990), Air-sea interaction, in *The Sea, Ocean Eng. Sci.*, vol. 9, edited by B. LeMehaute and D. M. Hanes, pp. 239–292, John Wiley, New York.
Donelan, M. A., J. Hamilton, and W. H. Hui (1985), Directional spectra of wind-generated waves, *Philos. Trans. R. Soc. London A*, *315*, 509–562.
Edson, J. B. (1990), Simulating droplet motion above a moving surface, in *Modeling the Fate and Influence of Marine Spray*, *Whitecap Rep. 7*, edited by P. Mestayer, E. C. Monahan, and P. A. Beetham, pp. 84–94, Univ. of Connecticut, Mar. Sci. Inst., Groton, Conn.
Emanuel, K. A. (1986), An air-sea interaction theory for tropical cyclones. Part 1: Steady-state maintenance, *J. Atmos. Sci.*, *43*(6), 585–605.
Emanuel, K. A. (1995), Sensitivity of tropical cyclones to surface exchange coefficients and revised steady-state model incorporating eye dynamics, *J. Atmos. Sci.*, *52*(22), 3969–3976.
Ezer, T., and G. L. Mellor (2004), A generalized coordinate ocean model and a comparison of the bottom boundary layer dynamics in terrain-following and in z-level grids, *Ocean Modell.*, *6*, 379–403.
Fairall, C. W., J. D. Kepert, and G. J. Holland (1994), The effect of sea spray on surface energy transports over the ocean, *Global Atmos. Ocean Syst.*, *2*, 121–142.
Fairall, C. W., E. F. Bradley, D. P. Rogers, J. B. Edson, and G. S. Young (1996), Bulk parameterization of air-sea fluxes for Tropical Ocean-Global Atmosphere Coupled-Ocean-Atmosphere Experiment, *J. Geophys. Res.*, *101*, 3747–3764.
Fox, D. N., W. J. Teague, C. N. Berron, M. R. Carnes, and J. M. Lee (2002), The modular ocean data assimilation system (MODAS), *J. Atmos. Oceanic Technol.*, *19*, 240–252.
Guan, C. L., W. Hu, J. Sun and R. L. Li (2007), The whitecap coverage model from breaking dissipation parameterizations of wind waves, *J. Geophys. Res.*, *112*, C05031, doi:10.1029/2006JC003714.
Han, G. J., W. Li, Z. X. F. Zhang, D. Li, Z. J. He, X. D. Wang, X. R. Wu, T. Yu, and J. R. Ma (2011), A regional ocean reanalysis system for China coastal waters and adjacent seas, *Adv. Atmos. Sci.*, *28*, 682–690.
Hasse, L. (1992), On the contribution of spray droplets to evaporation, *Boundary Layer Meteorol.*, *61*(3), 309–313.
Jarosz, E., D. A. Mitchell, D. W. Wang, and W. J. Teague (2007), Bottom-up determination of air-sea momentum exchange under a major tropical cyclone, *Science*, *315*(5819), 1707–1709.
Jeffrey, S. G., and M. F. William (2008), Effects of sea spray on tropical cyclones simulated under idealized conditions, *Mon. Weather Rev.*, *136*, 1686–1705.
Johnson, H. K., J. Hojstrup, H. J. Vested, and S. E. Larsen (1998), On the dependence of sea surface roughness on wind waves, *J. Phys. Oceanogr.*, *28*, 1702–1716.
Liu, B., C. L. Guan, and L. A. Xie (2012), The wave state and sea spray related parameterization of wind stress applicable from low to extreme winds, *J. Geophys. Res.*, *117*, C00J22, doi:10.1029/2011JC007786.
Lou, S. L., and H. Zhang (1995), Effects of spray on the momentum, heat and vapor transfers over the sea. II: Numerical calculations and comparison of results [in Chinese], *J. Ocean Univ. Qingdao*, *25*(2), 139–145.
Makin, V. K. (2005), A note on the drag of the sea surface at hurricane winds, *Boundary Layer Meteorol.*, *115*, 169–176.
Makin, V. K., and V. N. Kudryavtsev (1999), Coupled sea surface atmosphere model. 1: Wind over waves coupling, *J. Geophys. Res.*, *104*, 7613–7623.
Meirink, J. F., and V. K. Makin (2001), The impact of sea spray evaporation in a numerical weather prediction model, *J. Atmos. Sci.*, *58*(23), 3626–3638.

Miller, M. A. (1987), An investigation of aerosol generation in the marine planetary boundary layer, MS thesis, 142 pp., Dep. of Meteorol., Pennsylvania State Univ., University Park, Pa.
Monahan, E. C., and I. O'Muircheartaigh (1980), Optimal power-law description of oceanic whitecap coverage dependence on wind speed, *J. Phys. Oceanogr.*, *10*, 2094– 2099.
Park, J. J., Y. O. Kwon, and J. F. Price (2011), Argo array observation of ocean heat content changes induced by tropical cyclones in the north Pacific, *J. Geophys. Res.*, *116*, C12025, doi:10.1029/2011JC007165.
Perrie, W., E. L. Andreas, W. Q. Zhang, W. B. Li, and J. Gyakum (2005), Sea spray impacts on intensifying midlatitude cyclones, *J. Atmos. Sci.*, *62*, 1867–1883.
Powell, M. D., P. J. Vickery, and T. A. Reinhold (2003), Reduced drag coefficient for high wind speeds in tropical cyclones, *Nature*, *422*, 279–283.
Price, J. F. (1981), Upper ocean response to a hurricane, *J. Phys. Oceanogr.*, *11*, 153–175.
Riehl, H. (1954), *Tropical Meteorology*, 392 pp., McGraw-Hill, New York.
Reichl, B. G., T. Hara, and I. Ginis (2014), Sea state dependence of the wind stress over the ocean under hurricane winds, *J. Geophys. Res. Oceans*, *119*, 30–51, doi:10.1002/2013JC009289.
Rouault, M. P., and S. E. Larsen (1990), Spray droplet under turbulent conditions, *RISO-M-2845*, Dep. of Meteorol. and Wind Energy, RISO Natl. Lab., Denmark.
Rouault, M. P., P. G. Mestayer, and R. Schiestel (1991), A model of evaporating spray droplet dispersion, *J. Geophys. Res.*, *96*, 7181–7200.
Soloviev, A. V. R. Lukas, M. Donelan, B. K. Haus, and I. Ginis (2014), The air-sea interface and surface stress under tropical cyclones. *Sci. Rep.*, *4*, 5306 doi:10.1038/srep.
Toba, Y. (1972), Local balance in the air-sea boundary process. I: On the growth process of wind waves, *J. Oceanogr. Soc. Jpn.*, *28*, 109–120.
Uang, C. L. (1999), Impact of sea spray and oceanic on the development of tropical cyclones. Preprints, 23rd Conference on Hurricanes and Tropical Meteorology, Dallas, TX, pp. 30–31, Am. Meteorol. Soc., San Diego, Calif.
Wang, X. D., W. Li, Y. Q. Qi, and G. J. Han (2012), Heat, salt and volume transport by eddies in the vicinity of the Luzon strait, *Deep Sea Res., Part I*, *61*, 21–33.
Wang, Y. M., J. D. Kepert, and G. J. Holland (2001), The effect of sea spray evaporation tropical cyclone boundary layer structure and intensity, *Mon. Weather Rev.*, *129*, 2481–2500.
Wu, J. (1974), Evaporation due to spray, *J. Geophys. Res.*, *79*(27), 4107–4109.
Wu, J., J. J. Murray, and R. J. Lai (1984), Production and distributions of sea spray, *J. Geophys. Res.*, *89*, 8163–8169.
Zhang, H., and S. L. Lou (1995), Effects of spray on the momentum, heat and vapor transfers over the sea. I: Equations and initial values, *J. Ocean Univ. Qingdao*, *25*(2), 131–138.
Zhang, L. X., X. F. Zhang, G. J. Han, X. R. Wu, X. J. Cui, C. X. Shao, C. J. Sun, X. S. Zhang, X. D. Wang, and H. L. Fu (2015a), Impact of sea spray on upper ocean temperature during typhoon passage: Simulation with a 1-D turbulent model, *Chin. J. Oceanol. Limnol.*, *32*(5), 1164–1180.
Zhang, L. X., C. L. Guan, C. J. Sun, S. Y. Gao, and S. M. Yu (2015b), Upper ocean thermal response to sea spray mediated turbulent fluxes during typhoon passage, *Adv. Meteorol.*, *2015*, ID: 752947, doi:10.1155/2015/752947.
Zhang, X. F., G. J. Han, D. X. Wang, W. Li, and Z. J. He (2011), Effect of surface wave breaking on the surface boundary layer of temperature in the Yellow Sea in summer, *Ocean Modell.*, *38*, 267–279.
Zhang, X. F., G. J. Han, D. X. Wang, Z. A. Deng, and W. Li (2012), Summer surface layer thermal response to surface gravity waves in the Yellow Sea, *Ocean Dyn.*, *62*, 983–1000.
Zhang, W., and W. Perrie (2008), The influence of air-sea roughness, sea spray and storm translation speed on waves, *J. Phys. Oceanogr.*, *38*, 817–839.
Zhang, W., W. Perrie, and W. Li (2006), Impacts of Waves and Sea Spray on Midlatitude Storm Structure and Intensity, *Mon. Weather Rev.*, *134*, 2418–2442.
Zhao, D. L., and Y. Toba (2001), Dependence of whitecap coverage on wind and wind-wave properties, *J. Phys. Oceanogr.*, *57*(5), 603–616.